Halogens in serpentinised-troctolites from the Atlantis Massif: implications for alteration and global volatile cycling

Mark A Kendrick, Michael a W Marks, Marguerite Godard

Halogens in serpentinised-troctolites from the Atlantis Massif: implications for alteration fluids and global volatile cycling

Mark A. Kendrick[1], Michael A. W. Marks[2], Marguerite Godard[3]

1 - The School of Earth and Environmental Sciences, The University of Queensland, Brisbane, Qld. 4072, Australia **(ORCID 0000-0002-6541-4162)**

2 – Department of Geosciences, Eberhard Karls Universität Tübingen, Schnarrenbergstraße 94–96, 72076 Tübingen, Germany

3 – Géosciences Montpellier, Univ. Montpellier, CNRS, Montpellier, France **(ORCID 0000-0003-3097-5135)**

Words = 4745

Abstract: The concentrations of halogens in serpentinised olivine-rich lithologies in the lower oceanic crust (e.g. troctolites and wehrlites) are contrasted with altered-gabbros recovered from IODP Hole U1309D on the Atlantis Massif of the Mid-Atlantic Ridge. The aims are to evaluate if serpentinisation of lower crustal lithologies could significantly contribute to subduction-zone volatile budgets and if serpentinites formed from seawater preserve seawater-like halogen signatures. The olivine-rich lithologies are variably serpentinised by lizardite with minor chrysotile. The maximum concentrations of halogens in the most strongly serpentinised samples are 70 μg/g F, 2,100 μg/g Cl, 9,800 ng/g Br and 8 ng/g I. In comparison, the maxima in interlayered gabbros are 200 μg/g F, 130 μg/g Cl, 400 ng/g Br and 9 ng/g I. The Br/Cl ratios of the altered gabbros are strongly influenced by the presence of amphibole, which preferentially incorporates the smaller halides. The serpentinised lithologies have low F/Cl ratios, due to their strong enrichment in seawater-derived Cl, and they have Br/Cl and I/Cl ratios intermediate of unaltered crust and seawater-derived fluids. Seawater Br/Cl and I/Cl ratios are best preserved in the most Cl-rich samples consistent with these ratios fingerprinting the fluid responsible for serpentinization. Serpentinites formed from seawater in the lower ocean crust and lithosphere are likely to have low I/Cl ratios. Serpentinzed lithologies in the lower crust (and mantle lithosphere) could therefore significantly contribute to halogen subduction helping to explain the range of I/Cl ratios in arc lavas and a proposed decrease of mantle I/Cl over time.

Keywords: ocean crust, alteration fluid, fluorine, chlorine, bromine, iodine.

Introduction

Serpentinites form by the hydration of olivine- and orthopyroxene-rich ultramafic lithologies. Serpentinization of the ocean crust is of wide interest because serpentinization produces abiogenic hydrocarbons that can sustain chemotrophic ecosystems deep within the oceanic crust (e.g. Kelley et al., 2005, 2007; Bradley and Summons, 2010; Boreham et al., 2021) and serpentinites have the potential to dominate subduction-zone budgets of water and several groups of fluid mobile and volatile elements, including halogens, boron and noble gases (e.g. Rüpke et al., 2004; Scambelluri et al., 2004; Sharp and Barnes, 2004; Kendrick et al., 2011; 2017; Tonarini et al., 2011). The importance of serpentinites during subduction comes from their high concentrations of water (~13 wt %) and fluid mobile elements (e.g. ~0.1-0.5 wt % Cl), and the large stability field of serpentine polymorphs (Ulmer and Trommsdorff, 1995; Rüpke et al., 2004; Scambelluri et al., 2004; Sharp and Barnes, 2004; Kendrick et al., 2011). Antigorite, the high-pressure polymorph of serpentine, is stable to depths of more than 200 km on cold subduction geotherms (Ulmer and Trommsdorff, 1995). This means that serpentinised lithologies in the lower crust and lithosphere have the potential to transport significant water and Cl to sub-arc depths, and the partially dehydrated residues formed by antigorite breakdown, might recycle volatiles to even greater depths in the Earth's mantle (Rüpke et al., 2004; Kendrick et al., 2017; 2018b; Ohtani, 2020).

Serpentinites form in a variety of tectonic settings relevant to subduction (Deschamps et al., 2013): i) Seafloor serpentinites form from seawater interaction with abyssal peridotite or peridotite exposed on transform faults close to the seafloor. ii) Lithospheric mantle serpentinites underlying the ocean crust probably originate close to fractures penetrating the seafloor, and at the slab-bend where normal faults form on the outer rise and penetrate at

least ~25 km into the lithospheric mantle (Ranero et al., 2003; Grevemeyer et al., 2018). iii) Forearc serpentinites form from slab-fluids in the mantle wedge above the subducting slab (Bostock et al., 2002). iv) Subduction-melange serpentinites are suggested to form at the interface of the subducting slab and overriding mantle wedge where slab fluids that have interacted with multiple lithologies produce serpentinites with geochemical signatures inherited from dehydrating sediments and ocean crust (Marschall and Schumacher, 2012).

Previous studies of halogens in serpentinites have shown that in addition to Cl, serpentinites generally have high but variable concentrations of Br and I but relatively low concentrations of F (John et al., 2011; Kendrick et al., 2013b; Pagé and Hattori, 2017; Kendrick et al., 2018b; Pagé et al., 2018; Pagé and Hattori, 2019; Carter et al., 2021). Forearc serpentinites from the South Chamorro serpentine mud volcano in the Marianas, tectonic breccias in the Guatemala forearc, and many ophiolitic serpentinites, have Br/Cl and I/Cl ratios that are much higher than seawater and the mantle and encompass a range similar to pore waters in marine sediments (Kendrick et al., 2013b; Pagé et al., 2018; Carter et al., 2021). This led to the suggestion that serpentinites can preserve Br/Cl and I/Cl ratios of close to the serpentinizing fluid, meaning that halogen abundance ratios in serpentinites can help constrain the nature of fluids responsible for serpentinization (Kendrick et al., 2013b). However, the high I/Cl ratios of forearc serpentinites that are much higher than most arc lavas also means that forearc serpentinites are unlikely to be a major source of volatiles at sub-arc depths (Kendrick et al., 2020a).

In the current study we test the potential of serpentinized lithologies formed at a mid-ocean ridge without the influence of sediments to preserve Br/Cl and I/Cl ratios similar to seawater, which is the ultimate source of alteration fluids on the Atlantis Massif (e.g. Frost et

al., 2008; Beard et al., 2009; Roumejon et al., 2018; Ternieten et al., 2021). In addition, we evaluate the potential for serpentinization of olivine-rich lithologies in the lower crust to contribute to global volatile budgets. These are important questions because serpentinized-troctolites (and other olivine-rich lithologies) in the lower crust have not been included in subduction-budgets of the altered ocean crust previously (e.g. Ito et al., 1983; Jarrard, 2003; Sharp and Barnes, 2004; Chavrit et al., 2016). However, fractures formed in and around olivine as a result of volume expansion associated with serpentinization (Plümper et al., 2012) in olivine-rich lithologies could form permeable pathways in the lower crust that will be highly enriched in seawater-derived volatiles (e.g. Frost et al., 2008; Beard et al., 2009; Yoshida et al., 2020). The high I/Cl ratios typical of forearc serpentinites does not favour their involvement in subduction of halogens to sub-arc depths (Kendrick et al., 2020b). However, if serpentinites formed from seawater (without the influence of sediments) can preserve high concentrations of Cl and low I/Cl ratios, seafloor and lithospheric serpentinites could make major contributions to halogen subduction (e.g. Sharp and Barnes, 2004; Kendrick et al., 2011; 2013; 2018b; 2020a). Therefore this study tests the ability of serpentinized rocks to preserve fluid Br/Cl and I/Cl signatures and uses this knowledge to re-evaluate the most important types of serpentinite in global subduction-zone volatile cycles.

The Atlantis Massif

The Atlantis Massif is a ~1.5-2 Ma oceanic core complex that forms a bathymetric high at approximately 30°N on the western side of the Mid-Atlantic Ridge (Fig 1; Blackman et al., 2006). Its Southern Ridge reaches a minimum water depth of ~700 m, is dominated by peridotite and hosts the active serpentinite-hosted Lost City hydrothermal vent field (Kelley

et al., 2005; 2007). In contrast, the Central Dome, which was penetrated by the ~1400-m deep Hole U1309D of the Integrated Ocean Drilling Program (IODP), is dominated by gabbroic rocks typically associated with MORB differentiation, including olivine gabbros, gabbros, gabbronorites and more evolved oxide and leucocratic gabbros (Blackman et al., 2006). In addition, about 8% of the lithologies recovered from Hole U1309D are olivine-rich and include troctolites (30-70% olivine) interpreted as primitive olivine cumulates (~3% of recovered lithologies) and olivine-rich troctolites (>70% olivine), wehrlites and dunites (~5% of recovered lithologies) that could have formed by impregnation of mantle lithologies with basaltic melt (Expedition 304/305 Scientists, 2006; Drouin et al., 2009; Godard et al., 2009; Drouin et al., 2010).

Alteration shows an overall decrease down Hole U1309D but is strongly developed in the olivine-rich lithologies at all depths (Blackman et al., 2011). Previous studies of Hole U1309D lithologies have shown alteration records a range of temperatures extending from upper-amphibolite to sub-greenschist facies, reflecting alteration soon after initial emplacement, during exhumation and in an off-axis setting (Beard et al., 2009; Blackman et al., 2006; 2011; Nozaka and Fryer, 2011; Ternieten et al., 2021).

Sampling and methods

Representative 'gabbros' (gabbros and gabbronorites) and 'olivine-rich lithologies' (troctolites, olivine-rich troctolites and wehrlites) recovered from Hole U1309D during IODP Expeditions 304 and 305 were selected for geochemical analysis, with corresponding thin sections obtained from nearby sections of core in each unit (Expedition 304/305 Scientists, 2006). The shipboard thin sections were investigated for F and Cl by electron microprobe, and

related shipboard whole-rock powders were analysed for F and Cl by combustion ion chromatography and Cl, Br and I by the noble gas method (Kendrick, 2012; Kendrick et al., 2013a). Additional sample characterisation was undertaken by optical microscopy and Raman spectroscopy.

Electron microprobe analyses undertaken at the University of Queensland Centre for Microscopy and Microanalysis used a JEOL JXA-8200 superprobe. Conditions were optimised for F and Cl detection with an accelerating voltage of 15 kV, a probe current of 30 nA and a defocussed spot of 10 μm. F and Cl were analysed on dedicated channels using TAP and PET crystals, respectively, with counting times of 100 secs on peak and 90 secs on the backgrounds each side of the peaks (i.e. 280 secs total). The other elements were measured on the remaining 3 channels, Na was counted for 20 secs at the start of the measurement, with most other elements counted for 30 seconds. The measurement cycle of c. 5 mins was limited by measurement of F and Cl, which under these conditions had nominal detection limits of 20 μg/g Cl and 200 μg/g F, which approximates the uncertainty of all analyses. The elements were standardised against mineral standards including tugtupite with 7.6 wt. % Cl and MgF_2, measured at regular intervals throughout each session.

Micro-Raman spectroscopy was undertaken using a Renishaw Raman microscope and spectrometer at the University of Queensland Centre for Microscopy and Microanalysis. Minerals were targeted with a 514 nm laser focused to a ~2 μm spot size. Spectra were processed using the WiRE software version 4.4 and compared with reference spectra in the RRUFF database.

Fluorine and Cl concentrations were analyzed in ~10 mg sized aliquots of powdered sample by combustion ion chromatography at the Universität Tübingen using a 930 Compact

IC Flex chromatograph (Metrohm) connected to a combustion oven and autosampler (MMS 5000; Analytik Jena). Each sample was mixed with equal amounts of WO_3 (as a flux/promoter) and inserted into a quartz vial that was capped on both sides with quartz wool and placed into a glass vessel. The vessels where heated in an extraction line coupled to the IC to 1050 °C, maintaining a constant flow of Ar (6.0; 100 mL/min), O_2 (5.0; 300 mL/min), and water (0.2 mL/min). The loaded steam was collected in an absorber module containing 10 mL of 500 µg/g H_2O_2 solution and subsequently injected into the ion chromatograph equipped with a Metrosep A Supp 5-250/4.0 column. Calibration was achieved with a 6-point- quadratic calibration curve that covered the concentrations investigated and was constructed using the Metrohm intelligent Partial Loop Injection Technique (MiPT). Based on the frequent analyses of standard solutions, reference materials and replicates of the actual samples, relative uncertainties were generally <5% (1σ level).

Bromine and I concentrations were determined based on Br/Cl and I/Cl ratios measured by the noble gas method at the University of Queensland and the concentration of Cl measured by combustion ion chromatography. Br/Cl and I/Cl ratios were measured in ~10 mg-sized aliquots of sample powder in vacuated silica glass capsules that were irradiated together with the Hb3Gr ^{40}Ar-^{39}Ar flux monitor (Roddick, 1983) and aliquots of three scapolite halogen standards (Kendrick et al., 2013a; Kendrick et al., 2018a). The samples were irradiated in the central position of the McLellan Nuclear Research Center, UC Davis. Samples were included in a 40 hr irradiation on the 22nd August 2019, and received a total neutron fluence of 3.3×10^{18} neutrons cm^{-2} (Irradiation designated RS#6). Six sample duplicates were subsequently irradiated for 45 hrs on the 12th of October 2021 and received a total neutron fluence of 3.5×10^{18} neutrons cm^{-2} (Irradiation designated RS#8). Following each irradiation, irradiation-produced and naturally occurring noble gases were released by fusing the

vacuated silica glass capsules at 1600 °C in a ultra-high vacuum resistance furnace over a period of 20 mins. The noble gases released were purified on a Ti-foil getter during the heating step and using SAES getter pumps over a further period of 20 minutes. The purified noble gases were then admitted to the MAP 215-50 noble gas mass spectrometer and analysed for isotopes of Ar, Kr and Xe over 7 cycles of measurement. Br/Cl and I/Cl ratios were determined from the irradiation-produced noble gas proxy isotopes $^{80}Kr_{Br}/^{38}Ar_{Cl}$ and $^{128}Xe_{I}/^{38}Ar_{Cl}$ based on the noble gas production ratios determined from the scapolite standards. Unfortunately a delay between RS#6 and sample measurement meant that $^{37}Ar_{Ca}$ was not reliably measured, which precluded independent measurement of concentrations via internal standardisation to Ca. The precision of halogen ratio measurements depends on sample size, however, the scapolite standards included in multiple irradiations are reproducible at the 5% level for Br/Cl and 10% for I/Cl (2 s.d.) (Kendrick et al., 2013a; 2018a). Additional analytical details and data reduction protocols are available in Kendrick (2012) and Kendrick et al. (2018a).

Results

Petrography

The troctolites (20-70% olivine), olivine-rich troctolites (>70 % olivine) and wehrlites are much more strongly altered than the gabbro, gabbronorite or diabase samples. As reported previously, olivine is variably replaced by serpentine (Figs 2ab). Olivine in the least altered troctolites is cut by veinlets of serpentine that define mesh textures (Fig 2a; Beard et al., 2009). Magnetite is unevenly distributed along the central parts of some but not all serpentine veins (Fig 3a,bf). As the degree of serpentinisation increases the serpentine

veinlets become progressively wider and more numerous until kernel textures develop with only isolated olivine relicts (Figs 3a-c) or complete replacement of olivine (Fig 2b). In highly altered troctolites haloes of Mg-chlorite develop around plagioclase (Figs 2c-f) and plagioclase truncating serpentine veinlets is recrystallised and/or completely replaced by chlorite and prehnite (Figs 2b and 3a). In the most intense alteration, prehnite is replaced by hydrogrossular (Frost et al., 2008), and the combined prehnite-hydrogrossular alteration is associated with a distinctive Fe-rich chlorite (Fig 3a). This 'micro-rhodingite' alteration was described in detail by Frost et al. (2008). Rare blobs of primary chromite are preserved within olivine and plagioclase and sometimes surrounded by magnetite haloes.

Olivine in the wehrlite (140R2 50-56) is replaced by multiple generations of talc and cut by serpentine veinlets associated with iron sulphide rather than magnetite, and plagioclase has been almost completely replaced by two generations of Mg-chlorite halo (Fig 2 cd). The troctolitic-gabbro (91R2 81-92) has a modal abundance of only ~20 % olivine. The olivine is cut by serpentine veinlets and replaced by mixtures of talc and amphibole, with the amphibole present as a rim on olivine grain boundaries (Fig 3e). In places, patches of intergrown Mg-chlorite and amphibole result from the complete replacement of either olivine or clinopyroxene (Figs 2e,f and 3f). These textures were previously interpreted as olivine pseudomorphs based on the occurrence of tremolite rims on olivine associated with chlorite haloes (e.g. Nozaka and Fryer, 2011) (Fig 3e). However, tremolitic amphibole locally replaces clinopyroxene (Nozaka and Fryer, 2011) suggesting an origin from clinopyroxene is not precluded.

The least altered gabbros preserve abundant pristine plagioclase with scarce alteration minerals concentrated in fractures in and around olivine and orthopyroxene where

present. Sample 68R1-126/128 is the most strongly amphibolitised gabbro with green amphibole veins and abundant replacement of clinopyroxene (Fig 2gh). In addition to amphibole, clay minerals are present in the diabase sample (16R4 90-92), which comes from relatively high in the Hole.

Mineral chemistry

Representative compositions are reported for selected alteration minerals in the troctolites, olivine-rich troctolites and wehrlites in Table 1, and in the diabase, gabbros and gabbronorites in Table 2. Electron microprobe measurements are reported comprehensively in the electronic supplement.

Electron microprobe analyses of phyllosilicates are shown on an atomic basis in Figure 4. These data show that most serpentine analyses vary between pure serpentine and a mixture of ~90% serpentine and ~10% brucite (Fig 4) similar to that reported in other troctolite samples by Beard et al. (2009). Minerals identified as serpentine on textural grounds (e.g. veinlets defining mesh and kernel textures) have molar #Mg of 0.94 ± 0.04 [#Mg = Mg/(Mg +Fe)], and mostly contain less than 1 wt. % Al_2O_3 (Table 1; Fig 4). However, serpentine and talc (#Mg of 0.91 ± 0.07) are intergrown on a sub-micron scale in veinlets within some samples. Furthermore, a few analyses with elevated Al_2O_3, including the most Cl-rich serpentine veinlet investigated, represent either Al-rich serpentine (trending toward amesite) or nano-scale intergrowths of serpentine and chlorite (Fig 4a). As expected the serpentine and talc have #Mg substantially higher than the value of 0.84 ± 0.03 in the relict olivine, consistent with partitioning of Fe into magnetite.

Most chlorite in olivine-rich samples and gabbros is Mg-rich clinochlore or penninite with average #Mg of 0.86 ± 0.06 (Fig 4). However, chlorite varies toward Si-rich (talc-chlorite) in the talc altered wehrlite (140R2 50-53) and toward Fe-rich varieties (daphnite) with #Mg of less than 0.2 where troctolitic plagioclase is replaced by prehnite and hydrogrossular (Figs 3a and 4; Table 1). The chlorite and talc are intergrown with saponite on a nano-scale explaining the spread of the data in Fig 4a, and a correlation between the abundance of trace CaO and Al_2O_3 in talc (Supplementary data). Amphiboles are calcic with #Mg ranging from 0.9 to 0.2 (Fig 5). Tremolite dominates in the troctolites and olivine-rich troctolites (e.g. Fig 3 e,f), while actinolite, ferro-actinolite, hornblende and ferrohornblende are present in the gabbros. Brown coloured hornblendes and ferrohornblendes with up to 0.9-1.5 wt. % TiO_2 were found in gabbros 68R1 126-128 and 191R3 66-69.

Serpentine polymorphs and geothermometry

Raman spectra were collected for 105 points (2 μm spots) in 11 samples including the troctolitic gabbros, troctolites, olivine-rich troctolites and wehrlites and an olivine gabbro (221R3 91-99). Spectra were obtained for talc, chlorite and serpentine, which was investigated in all of its forms including: small magnetite-free veinlets (e.g. <10 μm wide); wider magnetite-free and magnetite-bearing veinlets; wider veins; and, patches of replacement. Of 64 serpentine spectra, 57 gave spectral features typical of lizardite or polygonal serpentine (Tarling et al., 2018; Fig 6); 2 spots in 136R2 57-60 and a single spot in 233R2 70-73 gave features similar to chrysotile (Fig 6); and 4 spots in 91R2 72-75 gave ambiguous weak responses that could have been chrysotile but are not distinguished in Fig 6. In most cases the OH-stretching peaks at 3680-3690 cm^{-1} are intermediate of the positions

reported for lizardite and chrystotile; and the subordinate peak that is characteristic of lizardite is shifted to values higher than the value of 3701 cm^{-1} reported as typical of lizardite (Tarling et al., 2018). The position of the OH-stretching peak intermediate of lizardite and chrysotile and the lack of a peak at 1045 cm^{-1} demonstrate the absence of antigorite. This includes in the earliest <10 µm wide magnetite-free veinlets in olivine, that are similar to those reported to contain antigorite in samples from core 227R3 (type I veins of Beard et al., 2009).

The lizardite and chrysotile polymorphs of serpentine are stable at temperatures of <300 °C indicating sub-greenschist facies conditions for serpentinization ofthe olivine-rich lithologies investigated. This is consistent with the composition of the Mg-chlorite present in haloes around plagioclase in the troctolite and wehrlite samples (Figs 2 and 3). Most Mg-chlorite in the troctolites and wehrliteshas 1.8-2.4 atoms of tetrahedral Al per 28 O, which according to the empirical calibration of hydrothermal chlorites by Cathelineau and Nieva (1985) and Cathelineau (1988), indicates formation temperatures of ~250-300 °C. The reliability of this thermometer is limited because it can also be influenced by bulk rock composition and the oxidation state of Fe (here assumed to be Fe^{2+}) (Hillier and Velde, 1991; Decaritat et al., 1993). However, the estimated temperatures of serpentinization and plagioclase alteration are consistent with the presence of magnetite and Mg-brucite (Fig 4) that indicate serpentinization at more than 200 °C (Klein et al., 2014); bulk-rock O-isotope data that supports average temperatures of more than ~200 °C (McCaig et al., 2010); and temperatures of ~200-300 °C previously indicated for the assemblage chlorite-actinolite-prehnite in Mg-rich metabasites (Frost et al., 2008; Starr et al., 2020). The chlorite-tremolite assemblage in the troctolitic gabbros (Figs 2e,f, and 3f) has previously been interpreted as forming at upper greenschist facies conditions (Blackman et al., 2006; Nozaka and Fryer,

2011). However, the alteration temperature is not tightly constrained and we question if compositionally similar Mg-chlorite haloes surrounding chlorite-tremolite patches in troctolitic gabbro (Fig 2 e, f) and surrounding plagioclase in troctolite (Fig 3a) might not have formed at similar temperature. In contrast with serpentinisation, the dominant alteration mineral in gabbroic rocks is green actinolitic amphibole, which undoubtedly formed at higher-temperature greenschist facies conditions (Fig 2gh; Blackman et al., 2006). Furthermore, brown hornblendes in sample 68R1 126-128 have maximum TiO_2 content of 1-1.4 wt.%, which equates to temperatures of ~700-800 °C based on the Ti in calcic-amphibole thermometer of Ernst and Liu (1998) indicating the preservation of some amphibole formed under high-temperature amphibolite facies or magmatic conditions. Therefore, the lithologies investigated record alteration minerals encompassing much of the Atlantis Massifs cooling history from amphibolite to sub-greenschist facies, with the gabbroic lithologies dominated by greenschist facies alteration and the troctolites, olivine-rich troctolites and wehrlites dominated by sub-greenschist facies alteration (Blackman et al., 2006).

Halogens in minerals

Most of the secondary minerals analysed have Cl concentrations of much higher than the electron microprobe detection limit of 20 µg/g Cl, meaning that Cl was reliably analysed. In contrast, many F measurements are close to the detection limit and have a minimum uncertainty of 200 µg/g meaning they are only indicative in spots with less than a few hundred µg/g F.

On average, serpentine in olivine-rich lithologies has the highest concentration of Cl in any of the minerals investigated (Fig 7). Serpentine has a mean and standard deviation in

all samples of 1900 ± 1600 μg/g Cl and a maximum of 1.2 wt. % Cl in a Al-rich serpentine (or serpentine-chlorite) veinlet in sample 70R2 39-43 (Fig 4a). The average concentration of Cl in serpentine varies between samples, serpentine contains ~400-1000 μg/g Cl in troctolite 23R2-89/101 compared to ~2000-4000 μg/g Cl in olivine-rich troctolite 256R2 90-92. Fluorine was below the electron microprobe detection limit (200 μg/g F) in most of the serpentine analysed (n = 209/220) implying serpentine has an average F/Cl ratio of less than ~0.1.

Talc has from a few 10's μg/g Cl to 1000 μg/g Cl, and a few hundred μg/g F were detected in some spots including talc in the wehrlite 140R2 50-53. Most chlorite, irrespective of #Mg contains <200 μg/g Cl but a handful of analyses have high concentrations in the 1000's of μg/g Cl range. Most prehnite and hydrogrossular contain <200 μg/g Cl. Tremolite associated with chlorite in the troctolitic gabbro 91R2 72-75 contains as little as 20-40 μg/g Cl and only a few hundred μg/g Cl in other troctolites, olivine-rich troctolites and wehrlites (Table 1; Electronic Supplement). Tremolite has variable F concentrations ranging from below the electron microprobe detection limit upto several hundred μg/g in the troctolitic gabbro 91R2 72-75 and the wehrlite 140R2 50-53. The relatively high F/Cl of the tremolite is consistent with crystal chemical controls that favour incorporation of F over Cl in Mg-rich amphiboles (e.g. Cl-Mg and F-Fe avoidance (Volfinger et al., 1985; Kullerud, 1996; Jenkins, 2019)).

The gabbros host amphibole with variable halogen abundance. Chlorine ranges from ~100-1000 μg/g in actinolites, upto ~200-3200 in μg/g Cl in hornblendes (Fig 5). Amphiboles with lower #Mg tend to have higher Cl concentrations, but the concentration of Cl varies by at least 1000 μg/g at any given #Mg (cf. Fig 5), which must result from variations in Cl activity related to the salinity of alteration fluids. Fluorine was above the electron microprobe

detection limit in the majority but not all of the actinolites and hornblendes analysed (supplementary data). The brown TiO_2-rich ferrohornblendes in gabbro 68R1 126-128 are among the most Cl and F rich with 1200-1500 μg/g Cl and 1500-3200 μg/g F. The high concentrations of F and Cl in the same ferrohornblendes cannot be explained by crystal chemical controls (F-Fe and Cl-Mg avoidance) but probably reflect the involvement of F and Cl-rich magmatic fluids during high temperature alteration, such as preserved in trondhjemite fluid inclusions (Castelain et al., 2013).

Halogens in whole rocks

The whole rock concentrations of F, Cl, Br and I in U1309D lithologies are reported in Table 3. The olivine-rich lithologies (troctolites, olivine-rich troctolites and wehrlites) have average concentrations and standard deviations of 26 ± 17 μg/g F, 720 ± 650 μg/g Cl, 2800 ± 3000 ng/g Br and 5 ± 2 ng/g I. In comparison, the gabbros and diabase have a higher average concentration of 56 ± 62 μg/g F and lower average concentrations of 65 ± 41 μg/g Cl, 130 ± 100 ng/g Br and 2 ± 2 ng/g I (Table 3).

The whole rock Cl concentration is plotted against the H_2O concentration in Fig 8 and is annotated with slopes showing the estimated ranges of H_2O/Cl ratios in the dominant alteration minerals with representative ranges of Cl concentration. The most Cl-rich troctolites and olivine-rich troctolites have H_2O/Cl ratios consistent with the dominance of Cl-rich serpentine with 3000-4000 μg/g Cl (Fig 8). In contrast, the wehrlite (140R2-11/19) and the troctolitic gabbro (91R2-81/90) have higher H_2O/Cl ratios influenced by talc, chlorite and tremolite (Fig 9). The gabbros and gabbronorites encompass a large range of H_2O/Cl ratios

reflecting the variability of amphibole Cl content (~100-2500 µg/g Cl) and the variable presence of talc or chlorite (Fig 9).

There is not a downhole trend with respect to Cl concentration in either the whole rocks, the serpentine or the amphibole (Fig 9). Rather the highest whole rock Cl concentrations and the highest serpentine Cl concentrations correspond to intervals with high abundances of olivine-rich lithologies (troctolites, olivine-rich troctlites or wehrlites) (cf. Figs 1 and 8).

Discussion

Halogen-enrichment

On average the olivine-rich lithologies (troctolites, olivine-rich troctolites and wehrlites) contain half as much F as the gabbroic lithologies but 11 times more Cl, 21 times more Br and 2 times more I (Table 3). In order to fully understand the variable halogen enrichment of the different lithologies it would be helpful to compare each lithology to an unaltered protolith. The alteration state of the recovered lithologies means that this is not possible, however, the halogen-enrichment of each lithology can be quantified by referencing the halogens to fluid-immobile trace elements of similar compatibility (Fig 10).

Previous work suggests that F has a compatibility in the mantle similar to Pr (or Nd) and Cl, Br and I have compatibilities in the mantle similar to Nb (e.g. le Roux et al., 2006; Le Voyer et al., 2015; Kendrick et al., 2017). Therefore the average F/Pr of 105 ± 25 (1 s.d) and the average Cl/Nb of 17 ± 10 (1 s.d.) in mid-ocean ridge and ocean island basalts (Kendrick et al., 2017) can be considered representative of both the mantle and unaltered oceanic crust.

Most of the Atlantis Massif gabbros have F/Pr 75-140 that are close to the expected range of unaltered oceanic crust. The olivine-rich lithologies have slightly higher values of 260-580 that suggest a factor of 2-6 times enrichment in F compared to unaltered oceanic crust or mantle (Fig 12a). In contrast with F, the gabbros have Cl/Nb of up to ~900 and the olivine-rich lithologies have Cl/Nb of up to ~12,000 that indicate Cl enrichment of up to ~50 times in the gabbros and of up to ~700 times in the olivine-rich lithologies relative to unaltered oceanic crust (Table 3).

The strong relative enrichment of Cl (~50-700 times) compared to F in all lithologies is consistent with alteration by seawater-derived fluids: F has a low solubility in seawater and seawater contains only 1.3 μg/g F compared to ~2 wt.% Cl (Seyfried and Ding, 1995; Drever, 1997). The slight enrichment of F in the olivine-rich lithologies (~0-6 times) compared to unaltered protoliths probably reflects remobilisation of F from the gabbros into the interlayered troctolites, olivine-rich troctolites and wehrlites at sub-greenschist facies conditions. Based on the measured concentrations of Pr in the different lithologies (Table 3), we would expect the gabbros to have had initial concentrations of F about 6 times higher than the more primitive olivine-rich lithologies that are more depleted in incompatible elements. Compared to the protoliths, the degree of Cl enrichment in the olivine-rich lithologies is about ten times greater than in the gabbros (Fig 10). This is explained by the high modal abundance of olivine in the olivine-rich lithologies, which is highly reactive and readily hydrated to form serpentine, and by the high Cl content of the serpentine.

Preserving seawater halogen signatures in serpentine

The whole rock halogen data define two distinct groups in the Br/Cl-I/Cl plot (Fig 11). The gabbro and gabbronorite samples, in which amphibole is the dominant Cl host, are displaced toward low Br/Cl and variable I/Cl ratios similar to those reported for amphibole in oceanic crust (Fig 11a; Kendrick et al., 2015a; 2019ab; Chavrit et al., 2016). The low Br/Cl and I/Cl ratios of the most Cl-rich amphibolitised gabbros is explained because the smaller Cl^- anion is preferentially incorporated into the small hydroxyl site within the amphibole structure, and the larger Br^- and I^- anions are preferentially excluded (Kendrick et al., 2015a). The relative compatibilities of Cl>Br>I in amphibole has been suggested previously because Cl-rich amphiboles have low Br/Cl ratios and associated high salinity fluid inclusions have high Br/Cl ratios (Svensen et al., 2001; Kendrick et al., 2015a).

In contrast to the gabbros, the olivine-rich lithologies, in which serpentine is the dominant alteration mineral, define a trend in the Br/Cl and I/Cl diagram that extends from the compositional range of pristine oceanic crust with mantle-like composition toward a second component with low I/Cl and a maximum Br/Cl of $(4.8 \pm 0.1)\times10^{-3}$ that is ~40% higher than seawater (Fig 11a). Importantly, the indicated trend away from the ocean crust is marked by increasing Cl concentrations consistent with the addition of seawater-derived Cl, Br and I in serpentine (Fig 11b).

The range of Br/Cl and I/Cl in the serpentinised lithologies is very unlikely to be explained by crystal chemical controls, because if crystal chemistry exerted a dominant control, all serpentinites would have similar ranges of Br/Cl and I/Cl (as observed for amphibole and amphibolitised ocean crust; cf. Fig 12). Instead, the serpentinised-lithologies have widely different Br/Cl and I/Cl ratios depending on where they formed. The serpentinised-troctolites in this study, which formed on a sediment-starved oceanic core

complex, have end-member Br/Cl and I/Cl ratios similar to seawater. In contrast, forearc serpentinites formed in subduction zones proximal to compacting sediments have Br/Cl and I/Cl ratios similar to sediment pore waters (Fig 12). The new data do not preclude the possibility that serpentine has a slightly higher preference for Br than Cl. However, given that alteration fluids in the ocean crust are commonly enriched in Br relative to Cl (Kendrick 2018; Kendrick et al., 2013a; 2015b; 2017), it seems more likely that the Br/Cl and I/Cl ratios of the serpentine are representative of a slightly modified seawater-derived alteration fluid (Figs 11 and 12). The involvement of modified seawater is also consistent with: i) the high and variable Cl content of the serpentine, which suggests the involvement of fluids with high but variable salinities rather than fresh seawater, and ii) the low abundance of brucite and the slight F-enrichment of the serpentinised lithologies, which are consistent with the alteration fluids introducing silica and F derived from previous equilibration with the surrounding gabbros, although significant silica would also have been derived from alteration of troctolitic plagioclase (Fig 3a; Beard et al., 2009).

The new data for the serpentinised-troctolites in this study support previous suggestions that Cl, Br and I are not strongly fractionated between fluids and serpentine and that serpentine Br/Cl and I/Cl ratios can be used to make inferences about the fluids involved in serpentinization (Kendrick et al., 2013b). The partitioning behaviour of halogens in serpentine have not been investigated experimentally. However, it is possible that Cl, Br and I are not strongly fractionated between fluids and serpentine because: i) the hydroxyl site in serpentine is somewhat larger and more open than in amphibole meaning it can more readily incorporate the larger anions; and ii) the layered structure of serpentine, which is commonly interlayered with brucite and other phyllosilicates and is known to sorb cations and organic contaminants (Carmigano et al., 2020) and might also sorb halogens.

Relatively few abyssal serpentinites have been analysed for Cl, Br and I previously. However, the existing data from other spreading centres and passive margins are consistent with serpentine recording fluid Br/Cl and I/Cl ratios. Four of the five serpentinites from mid-ocean ridges investigated previously record Br/Cl and I/Cl ratios within the range of fluid inclusions in Mathematician Ridge metagabbros (dark-red symbols in Fig 12; Kendrick et al., 2013; 2015). The fifth mid-ocean ridge serpentinite (S001) has anomalously high I/Cl that is not representative of serpentine but is explained by the presence of carbonate veins (Fig 12), which can be I-rich (Kendrick et al., 2019b; Kendrick et al., 2020a). The four abyssal serpentinites from passive margins have non-distinct Br/Cl and I/Cl signatures that overlap the mantle (unaltered crust) and sedimentary pore waters and probably reflect a long alteration history on the seafloor and an influence from sediments, which is seen even more strongly in ophiolites and in forearcs (Fig 12; see also Pagé and Hattori, 2017; Pagé et al., 2018).

Implications for global volatile budgets

Subduction-zone inputs based on estimating the alteration state of slabs entering subduction zones have a high uncertainty, because there are a limited number of analyses of samples of the lower ocean crust and the ocean crust is extremely heterogeneous (e.g. Ito et al., 1983; Hilton et al., 2002; Jarrard, 2003; Sharp and Barnes, 2004; Chavrit et al., 2016). The findings that serpentinised olivine-rich lithologies in the lower crust are much more strongly enriched in halogens than proximal gabbros and gabbronorites, and that they can preserve halogen signatures of close to the alteration fluid, have significant implications for understanding global halogen budgets (Figs 8, 9 and 11b).

Lower-crustal alteration

Previous budgets for halogens have included altered basalts and gabbros, but have not included olivine-rich lithologies in the lower crust (Ito et al., 1983; Jarrard, 2003; Chavrit et al., 2016). The proportion of troctolites in typical lower crust and the alteration state of these troctolites is poorly known. However, given that Hole U1309D on the Atlantis Massif has a bulk composition similar to primitive MORB (e.g. undifferentiated mantle melts) (Godard et al., 2009), the proportion of ~8% olivine-rich lithologies in Hole U1309D probably represents a minimum for typical ocean crust. This is because typically the crust underlying mid-ocean ridge basalts is depleted relative to primitive melts by basalt extraction, meaning a higher proportion of primitive cumulates is expected. It is not known if IODP Site U1415 (Hess Deep) on the East Pacific Rise is representative of typical lower ocean crust, however, troctolite cumulates comprise ~27% of the lithologies recovered from the crustal section at this site, which formed ~2 km beneath the sheeted dykes (Expedition 345 Scientists, 2013). Based on the average concentrations of Cl and H_2O in the gabbros and interlayered olivine-rich lithologies (troctolites, olivine-rich troctolites and wehrlites) in this study (Table 3), and the assumption that olivine-rich lithologies comprise ~10-20% of typical lower ocean crust, olivine-rich lithologies could easily host ~50-70% of the total Cl and H_2O in the lower ocean crust (Table 4).

Olivine-rich lithologies exhumed close to the seafloor on core complexes like the Atlantis Massif or in tectonic windows like Hess Deep are highly altered compared to nearby gabbros (Fig 8; Expedition 304/305 Scientists, 2006; Blackman et al., 2011; Expedition 345 Scientists, 2013; Schroeder et al., 2015; Nozaka et al., 2017). There is of course a question as to whether or not these lithologies are representative of olivine-rich lithologies within 'intact'

ocean crust, which might be less altered. However, two lines of reasoning suggest that olivine-rich lithologies in the lower crust entering subduction zones are likely to be highly altered. Firstly, even in the absence of brittle fractures, reactive troctolite layers within the ocean crust can form permeable pathways enabling the deep circulation of fluids in off axis settings (Yoshida et al., 2020). This is because serpentinization of olivine causes a volume change that can propagate fractures into the surrounding lithology (Plümper et al., 2012; Yoshida et al., 2020). Secondly, it is known that deep fractures formed at the slab-bend on the forearc bulge prior to subduction penetrate at least 25 km into the lithospheric mantle (Ranero et al., 2003; Grevemeyer et al., 2018). These fractures transect the crust providing ample opportunity for seawater, and more evolved higher-salinity seawater-derived fluids, to serpentinize the lower crust as well as the underlying lithospheric mantle.

Balancing inputs and outputs

The trace element signatures of arc lavas are commonly interpreted as indicating that a combination of sediment-melts and slab-fluids enrich the sub-arc mantle (e.g. Pearce and Stern, 2006). The slab-fluids are usually assumed to be derived from dehydration of subducting ocean crust and lithosphere, with serpentinites often suggested to make a large or dominant contribution (e.g. Scambelluri et al., 1995; Rüpke et al., 2004; Kendrick et al., 2011). However, Marschall and Schumacher (2012) proposed an intriguing alternative explanation for the mixed geochemical signatures of arc-lavas, suggesting that subduction melanges with a serpentinite matrix form at the slab-mantle interface enable physical mixing of crustal and sedimentary components. Melange diapirs then invade the overlying mantle

wedge and are melted to produce arc-lavas with chemical attributes inherited from both sediments and the oceanic crust (Marschall and Schumacher, 2012).

Geochemical arguments that support the melange diapir proposal based on radiogenic isotopes (Nielsen and Marschall, 2017) would be inconclusive if they allowed for the inherently variable nature of altered ocean crust. However, the melange diapir model is not favoured by the currently available halogen data, which suggests I-rich serpentinites such as those formed in forearcs and which are likely to dominate subduction melanges, are not an important source of halogens at sub-arc depths (Kendrick et al., 2014; 2020b). This is because serpentinites associated with sediments typically have I/Cl ratios that are much higher than arc lavas and the MORB mantle (Fig 12). Subduction of I-rich serpentinites is also unable to explain the suggested decrease in mantle I/Cl over Earth history, which is a result of preferentially subducting Cl relative to I (Kendrick et al., 2020b).

The current study confirms that serpentinites formed by interaction of seawater with olivine-rich lithologies in the crust or mantle can have low I/Cl ratios (Figs 11 and 12). Therefore, the relatively low I/Cl ratios of arc lavas that are lower than forearc serpentinites, and the proposed evolution of mantle I/Cl to lower values over Earth history (Kendrick et al., 2020), are consistent with subduction of halogens in serpentinised lithologies in the lower ocean crust and mantle lithosphere. The available halogen data therefore suggest that subduction of halogens (and other volatiles) in lower crustal and lithospheric serpentinites is more important than subduction of volatiles in forearc serpentinites or subduction melanges.

Conclusions

Olivine-rich lithologies in the Atlantis Massif are strongly but variably serpentinized by lizardite with minor chrysotile. Serpentine is by far the dominant host of Cl with an average concentration of ~1900 μg/g. Previous crustal inventories of H_2O, Cl, noble gases and other volatiles that did not include olivine-rich lithologies in the lower crust significantly underestimated (e.g. by ~50 %) the total abundance of these elements in the ocean crust.

Troctolites are on average ~10 times more enriched in Cl than interlayered gabbros and represent a major reservoir of H_2O and halogens in the lower crust. Serpentine minerals preserve Br/Cl and I/Cl ratios of close to the serpentinising fluids and indicate the dominance of seawater-derived fluids in serpentinization of Hole U1309D lithologies. Fluorine is only weakly enriched in alteration lithologies because it has a low concentration in seawater.

The involvement of I-rich sedimentary pore waters in serpentinization of forearcs and the association of subduction-melange serpentinites with sediments means they are unlikely to significantly contribute to halogen subduction. In contrast, seawater serpentinization could generate serpentinites with low I/Cl ratios either close to the seafloor or at the slab-bend. Subduction of lower crustal and lithospheric serpentinites with I/Cl ratios similar to Atlantis Massif troctolites could explain the range of I/Cl in arc lavas and significantly contribute to halogen subduction.

Acknowledgements

We thank the International Ocean Discovery Program (IODP) for providing the samples for the current study. This research was supported by the Australian Government through the Australian Research Council's *Discovery Projects* funding scheme (project DP180100580).

The authors acknowledge the facilities, and the scientific and technical assistance, of the Microscopy Australia Facility at the Centre for Microscopy and Microanalysis (CMM), The University of Queensland.

Table 1. Selected minerals in Hole U1309D troctolites, olivine-troctolites and wehrlites

	23R2-89/101	70R2-39/43	70R2-39/43	189R3-103/105	256R2-90/92	91R2-72/75	140R2-50/53	264R4-65/67	91R2-72/75	256R2-90/92
			Serpentine				Talc		Amphibole	
	n = 16	n = 23	n = 4	n = 41		n = 25	n = 23	n = 13	n = 24	n = 3
SiO_2	41.5 ± 0.7	41.0 ± 0.9	32.0 ± 2.5	41.6 ± 0.4	38.3 ± 2.5	58.0 ± 3.9	59.3 ± 3.8	55.4 ± 3.4	56.9 ± 0.9	41.5 ± 0.7
Al_2O_3	0.2 ± 0.7	0.5 ± 0.4	10.8 ± 2.8	0.2 ± 0.3	0.7 ± 1.6	0.4 ± 0.7	0.5 ± 1.2	0.7 ± 0.6	0.8 ± 0.5	13.0 ± 1.3
TiO_2										0.10 ± 0.01
FeO*	2.9 ± 1.7	1.9 ± 0.6	3.8 ± 2.2	2.8 ± 1.0	6.4 ± 3.1	3.0 ± 2.3	4.2 ± 2.2	10.1 ± 4.9	3.2 ± 1.1	16.9 ± 0.9
Fe_2O_3										
MnO							0.09 ± 0.08	0.1 ± 0.1	0.14 ± 0.04	0.9 ± 0.2
MgO	39.1 ± 2.1	40.1 ± 0.6	33.7 ± 3.3	39.0 ± 1.0	37.7 ± 1.6	28.7 ± 2.3	28.0 ± 3.0	24.2 ± 3.1	22.6 ± 1.0	7.34 ± 0.5
CaO			0.22 ± 0.11		0.1 ± 0.3	0.1 ± 0.1	0.4 ± 0.9	0.6 ± 0.5	12.7 ± 0.7	14.9 ± 0.3
K_2O									0.01 ± 0.01	0.10 ± 0.03
Na_2O		0.06 ± 0.03		0.04 ± 0.03	0.1 ± 0.1	0.11 ± 0.06	0.14 ± 0.11		0.18 ± 0.09	2.1 ± 0.2
NiO	0.2 ± 0.2	0.07 ± 0.04	0.09 ± 0.06	0.04 ± 0.04	0.2 ± 0.1	0.16 ± 0.05	0.13 ± 0.05		0.09 ± 0.03	
Total	84.1 ± 2.6	83.8 ± 0.7	81.5 ± 1.7	83.8 ± 0.8	83.9 ± 1.2	90.6 ± 2.6	92.8 ± 1.8	91.4 ± 3.0	96.7 ± 0.6	96.7 ± 0.7
F µg/g	b.d.	b.d.	b.d	b.d.	b.d.	b.d-380	b.d.-850	b.d.	600 ± 300	b.d.
Cl µg/g	690 ± 230	2900 ± 2200	10,000 ± 1800	1500 ± 500	3000 ± 1300	120 ± 50	80 ± 60	190 ± 200	50 ± 20	550 ± 100
#Mg	0.96 ± 0.02	0.97 ± 0.01	0.94 ± 0.4	0.96 ± 0.01	0.91 ± 0.04	0.95 ± 0.04	0.92 ± 0.04	0.81 ± 0.09	0.93 ± 0.03	0.44 ± 0.01

Data represent the average of 'n' analyses and 1 standard deviation

Table 1. continued

	23R2-89/101	91R2-72/75	256R2-90/92	70R2-39/43	256R2-90/92	23R2-89/101	70R2-39/43	100R1-48/50	100R1-48/50	256R2-90/92
	Mg-Chlorite			Fe-Chlorite		Prehnite			Hydrogrossular	
	n = 17	n = 41	n = 9	n = 8	n = 10	n = 3	n = 1	n = 5	n = 6	n = 2
SiO_2	31.7 ± 1.9	31.4 ± 2.3	30.6 ± 1.8	23.7 ± 0.5	27.2 ± 1.8	42.4 ± 0.4	43.2	42.6 ± 0.5	35.1 ± 1.3	33.2 ± 0.7
Al_2O_3	16.3 ± 2.6	17.2 ± 2.0	15.2 ± 2.1	22.6 ± 0.9	20.5 ± 1.4	23.8 ± 0.5	23.6	24.3 ± 0.5	21.6 ± 0.7	27.3 ± 0.1
TiO_2		0.01 ± 0.01				0.01 ± 0.01	0.01	0.03 ± 0.03		
FeO	5.1 ± 0.7	9.1 ± 2.8	12.4 ± 3.5	31.2 ± 3.0	21.3 ± 1.6	0.4 ± 0.4	0.3	0.4 ± 0.3	4.1 ± 2.6	0.16 ± 0.1
MnO	0.07 ± 0.02	0.14 ± 0.11	0.2 ± 0.1	2.4 ± 0.6	0.5 ± 0.1	0.06 ± 0.05	0.2	0.1 ± 0.1	1.2 ± 0.2	
MgO	30.5 ± 1.0	27.3 ± 2.3	25.8 ± 3.3	5.8 ± 1.4	16.0 ± 2.3	0.1 ± 0.1	0.01	0.01 ± 0.01	0.7 ± 0.8	
CaO	0.1 ± 0.3	0.2 ± 0.3	0.07 ± 0.03		0.9 ± 1.6	25.9 ± 0.4	25.8	25.9 ± 0.5	32.6 ± 2.8	30.5 ± 0.5
K_2O	0.12 ± 0.05	0.03 ± 0.03	0.02 ± 0.01		0.03 ± 0.02			0.02 ± 0.01		
Na_2O	0.04 ± 0.02	0.06 ± 0.08			0.2 ± 0.2	0.05 ± 0.05	0.1	0.04 ± 0.02		
NiO	0.08 ± 0.03	0.14 ± 0.09								
Total	84.1 ± 0.7	85.6 ± 1.1	84.6 ± 0.6	86.0 ± 0.7	86.7 ± 1.3	92.7 ± 0.1	93.3	93.4 ± 0.1	95.4 ± 1.3	92.2 ± 0.3
F µg/g	b.d.-600	b.d.	b.d.	b.d.	b.d.	b.d.	b.d.	b.d.	b.d.	b.d.
Cl µg/g	160 ± 70	110 ± 100	390 ± 50	240 ± 280	210 ± 50	60 ± 40	40	110 ± 70	110 ± 20	120
#Mg	0.91 ± 0.01	0.84 ± 0.05	0.78 ± 0.07	0.25 ± 0.06	0.57 ± 0.05					

Data represent the average of 'n' analyses and 1 standard deviation

Table 2. Selected minerals in Hole U1309D diabase, gabbros and gabbronorites

	16R4-113/116	68R1-126/128	68R1-126/128	191R3-66/69	264R1-65/67	16R4-113/116	264R1-65/67	221R3-100/102	264R1-65/67	277R2-96/98
	Amphibole					Chlorite		Serpentine	talc	Ilmenite
	n = 10	n = 14	n = 25	n = 32	n = 7	n = 7	n = 4	n = 4	n = 13	n = 5
SiO_2	51.3 ± 1.9	47.7 ± 0.7	50.7 ± 2.2	51.9 ± 1.9	51.4 ± 1.4	30.1 ± 1.6	32.6 ± 3.2	42.1 ± 0.3	55.4 ± 3.4	
Al_2O_3	3.6 ± 1.5	4.6 ± 0.5	2.7 ± 1.4	3.8 ± 1.3	4.0 ± 1.2	15.4 ± 0.9	16.3 ± 2.3	0.01 ± 0.01	0.7 ± 0.7	
TiO_2	0.4 ± 0.3	1.2 ± 0.2	0.18 ± 0.09	0.3 ± 0.4	0.3 ± 0.1					49.1 ± 0.9
FeO	14.9 ± 3.1	22.5 ± 0.5	21.8 ± 4.4	13.4 ± 2.9	14.0 ± 2.1	29.2 ± 1.2	9.6 ± 2.0	2.2 ± 0.3	10.1 ± 4.9	45.0 ± 1.1
MnO	0.2 ± 0.1	0.35 ± 0.05	0.4 ± 0.1	0.28 ± 0.08	0.3 ± 0.1	0.18 ± 0.03	0.07 ± 0.03	0.02 ± 0.01		
MgO	13.9 ± 2.2	9.1 ± 0.32	9.9 ± 3.3	15.4 ± 2.3	15.1 ± 1.5	11.2 ± 0.5	27.4 ± 1.9	40.3 ± 0.2	24.2 ± 3.1	1.2 ± 0.3
CaO	11.3 ± 1.3	9.7 ± 0.4	10.3 ± 1.6	11.2 ± 0.6	10.8 ± 1.0	1.0 ± 0.5	0.09 ± 0.02	0.04 ± 0.02	0.6 ± 0.5	1.6 ± 0.9
K_2O	0.1 ± 0.1	0.4 ± 0.1	0.06 ± 0.08	0.03 ± 0.03	0.04 ± 0.01	0.04 ± 0.02	0.1 ± 0.1	0.02 ± 0.01	0.07 ± 0.03	
Na_2O	0.7 ± 0.3	1.5 ± 0.1	0.5 ± 0.2	0.6 ± 0.2	0.7 ± 0.2	0.18 ± 0.05	0.14 ± 0.05	0.2 ± 0.2	0.2 ± 0.1	
NiO								0.12 ± 0.04		
Cr_2O_3										
Total	96.6 ± 0.3	97.1 ± 0.3	96.5 ± 0.8	97.1 ± 0.3	96.6 ± 0.3	87.3 ± 1.3	86.4 ± 1.4	85.0 ± 0.3	91.4 ± 3.0	97.2 ± 0.4
F µg/g	1200 ± 1000	2200 ± 500	620 ± 250	660 ± 420	b.d	b.d.	b.d.	b.d.	b.d.	b.d
Cl µg/g	820 ± 950	1300 ± 160	440 ± 360	530 ± 350	420 ± 130	110 ± 40	210 ± 50	760 ± 290	190 ± 200	b.d
#Mg	0.62 ± 0.08	0.42 ± 0.01	0.44 ± 0.13	0.67 ± 0.08	0.66 ± 0.05	0.41 ± 0.02	0.57 ± 0.05	0.970 ± 0.004	0.81 ± 0.09	-

Data represent the average of 'n' analyses and 1 standard deviation

Table 3. Whole rock halogen data for Hole U1309D lithologies

Sample	Lithology	#Mg	Pr µg/g	Nb µg/g	F µg/g	Cl µg/g	Br ng/g	I ng/g	H_2O wt. %	CO_2 wt. %	F/Cl	Br/Cl	I/Cl
'Olivine-rich lithologies'													
23R2-95/97	Troctolite	0.90	0.063	3.324	19	134	481	3.6	5.5	0.09	0.14	3.6 ± 0.3	27 ± 19
70R2-43/53	Troctolite	0.84	n.d.	0.086	17	2,100	9,760	7.8	8.3	0.05	0.01	4.6 ± 0.4	3.7 ± 1.6
91R2-81/90	Troct. Gabbro	0.83	0.139	6.405	36	87	239	1.7	2.1		0.41	2.8 ± 0.3	20 ± 4
100R1-50/55	Troctolite	0.86	0.091	0.151	29	846	3,960	6.9	3.9	0.09	0.03	4.7 ± 0.1	8.1 ± 1.8
111R3-131/138	Troctolite	0.87	0.033	0.126	19	1,680	6,840	4.8	6.3	0.09	0.01	4.1 ± 0.1	2.9 ± 0.2
189R3-67/76	Troct. Gabbro	0.83	0.279	0.153	23	188	707	3.6	1.1	0.06	0.12	3.8 ± 0.1	19 ± 9
232R3-110/117	Troctolite	0.85	0.060	0.624	16	867	2,720	6.2	7.3	0.12	0.02	3.1 ± 0.1	7.2 ± 4.1
234R2-63/68	Ol-rich Troctolite	0.85	0.029	0.129	17	615	1,890	6.4	5.6	0.13	0.03	3.1 ± 0.1	10 ± 2
256R2-88/94	Ol-rich Troctolite	0.84	0.029	0.176	16	695	2,050	6.7	4.5	0.10	0.02	3.0 ± 0.3	10 ± 8
Wehrlites				n.d.									
136R2-4/14	Wehrlite	0.86	0.068	b.d.l.	23	528	1,700	4.8	6.6	0.14	0.04	3.21 ± 0.04	9 ± 2
140R2-11/19	Wehrlite	0.82	0.332	0.478	74	228	323	3.4	8.2	0.75	0.32	1.4 ± 0.4	15 ± 1
'Gabbros'													
16R4-90/92	Diabase	0.49	2.371	3.324	179	126	184	9.4	1.0	<0.04	1.42	1.5 ± 0.1	74 ± 21
68R3-47/60	Gabbro	0.79	0.172	0.086	38	26	51	1.3	0.74	<0.04	1.49	2.0 ± 0.2	51 ± 34
113R2-7/22	Oxide Gabbro	0.28	2.975	6.405	197	128	162	1.0	0.56		1.53	1.3 ± 0.1	8 ± 4
145R1-64/74	Gabbro	0.72	0.271	0.151	40	70	149	0.7	0.59		0.58	2.1 ± 0.2	10 ± 15
162R3-71/86	Gabbro	0.74	0.243	0.126	29	40	82	1.1	0.92	0.07	0.71	2.0 ± 0.3	27 ± 23
172R3-41/51	Gabbro	0.77	0.183	0.153	25	68	114	1.8	1.4		0.37	1.7 ± 0.2	25 ± 22
191R3-55/66	Gabbronorite	0.69	0.735	0.624	41	88	175	1.1	0.26	0.04	0.47	2.0 ± 0.2	13 ± 3
212R4-72/78	Ol. Gabbronorite	0.75	0.202	0.129	27	21	19	0.4			1.31	0.9 ± 0.2	21 ± 12
221R3-91/99	Olivine Gabbro	0.78	0.182	0.176	17	26	42	1.4	0.24	0.06	0.65	1.6 ± 0.9	54 ± 62
255R1-28/35	Olivine Gabbro	0.81	0.111	n.d.	23	109	404	2.0	0.94	0.06	0.21	3.7 ± 0.2	19 ± 65
264R1-52/60	Gabbronorite	0.62	0.265	b.d.l.	28	66	160	2.3	0.42	0.06	0.42	2.4 ± 0.1	34 ± 9
277R2-96/106	Gabbro	0.76	0.423	0.478	28	17	48	2.0	0.49		1.68	2.9 ± 0.8	120 ± 80
Reference	Seawater										0.0001	3.5	~3.5

Uncertainties reported for Br/Cl and I/Cl represent either the 2σ analytical uncertainty or 2 standard errors where two aliquots were analysed. #Mg, Pr and Nb data are from Godard et al 2009

Table 4. Estimated proportion of Cl and H_2O in troctolites in the lower crust*

Proportion of Troct:Gab	% Cl in troctolites	% H_2O in troctolites
5:95	37	29
10:90	55	47
15:85	66	58
20:80	73	66

**Based on the average concentrations of H_2O and Cl in troctolitic and gabbroic samples in this study (Table 3)*

Fig 1 Kendrick et al., 2022

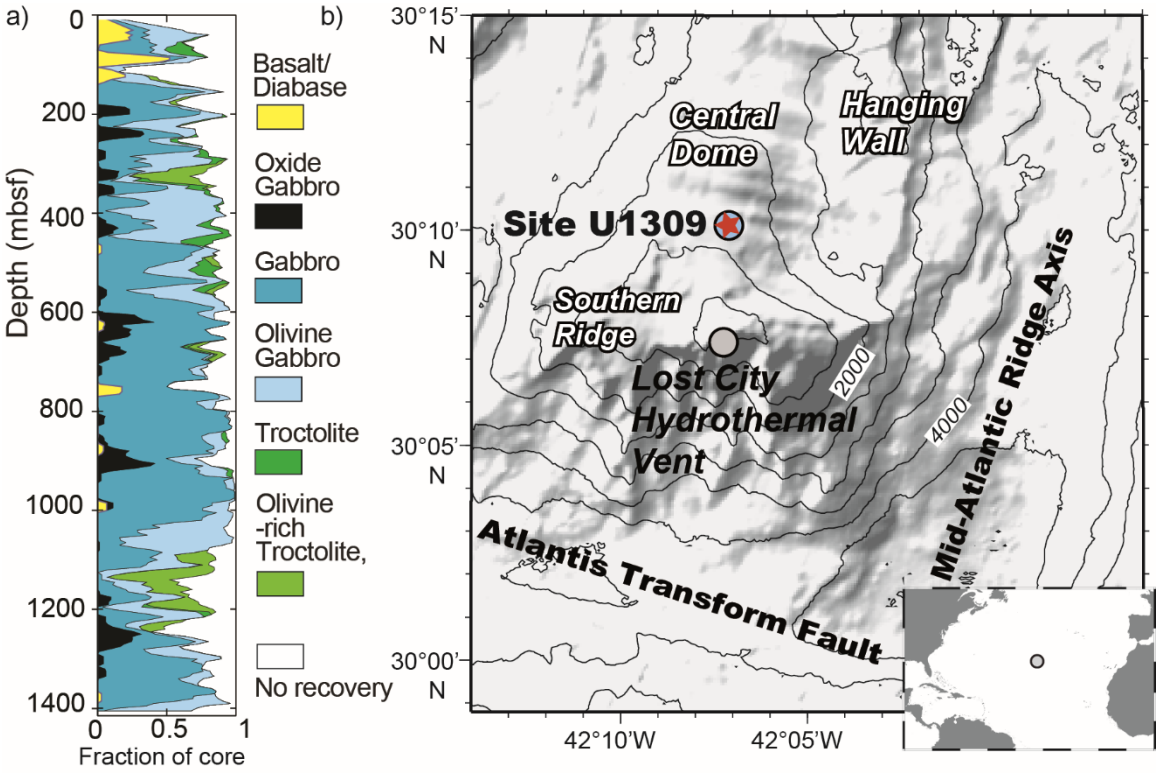

Fig 1. IODP Hole U1309D. a) Downhole plot showing a 20 m running average of the lithologies recovered from the hole; and b) a locality map showing the position of the Atlantis Massif on the Mid-Atlantic Ridge. Note that wehrlites and dunites are included with olivine-rich troctolites in panel a (adapted from Godard et al., 2009).

Fig 2 Kendrick et al., 2022

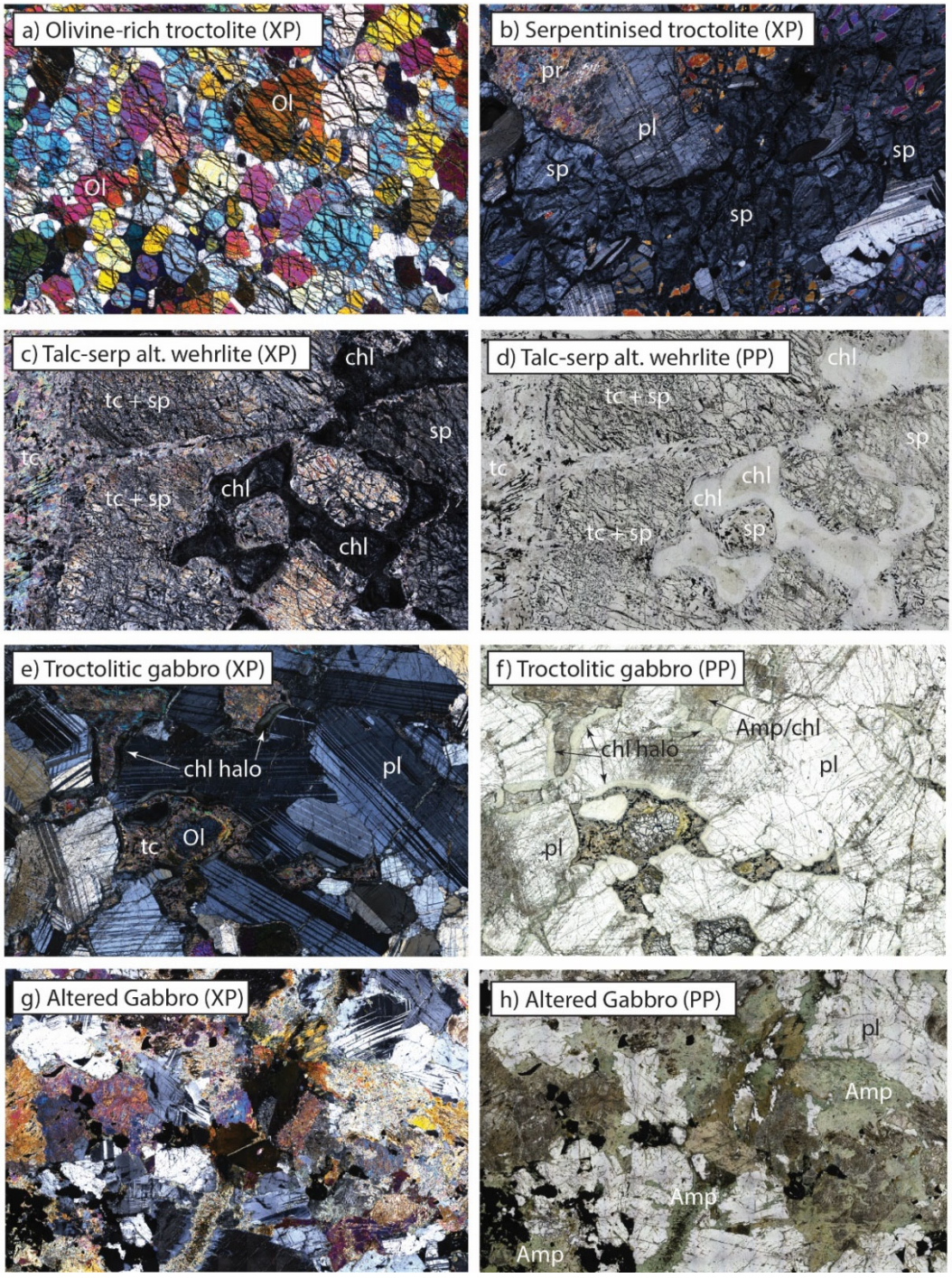

Fig 2. Representative examples of serpentinised troctolites and amphibolitised gabbro from Hole U1309D. a-b) cross polarised view of olivine-rich troctolite 256R2-90/92 in which olivine is cut by meshes of serpentine and magnetite and 70R2-39/43 in which olivine is largely replaced by serpentine and plagioclase is being replaced by prehnite. c-d) cross polar and plane polar view of 140R2-50/56 (wehrlite). Olivine is completely replaced by talc, which is cut by oxide-bearing serpentinite veinlets. Chlorite forms haloes around former plagioclase. e-f) Cross polar and plane polar view of troctolitic gabbro 91R2-72/75 . Chlorite haloes surround plagioclase, relicts of olivine are surrounded by talc replacement and patches of tremolite and chlorite have completely replaced former olivine or clinopyroxene (see also Figs 4e and f). g-h) cross polar and plane polar view of 68R1-126 (amphibolitised gabbro).

Fig 3 Kendrick et al., 2022

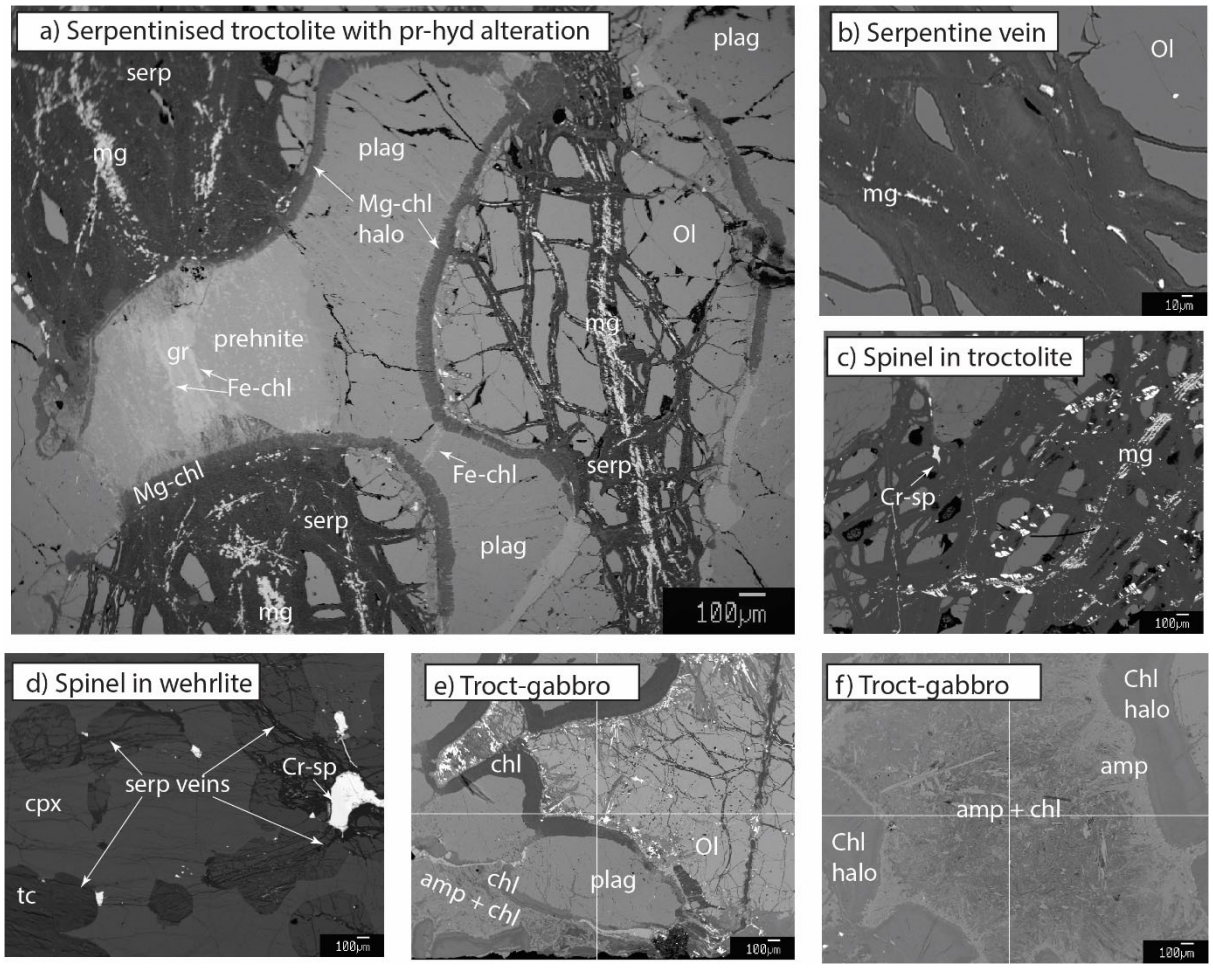

Fig 3. Back scattered electron images of alteration in troctolites. a-c) serpentinised olivine in samples 100R1-48/50 and 256R2-90/92. d) serpentine veinlets cutting pseudomorphs of olivine dominated by talc in wehrlite 136R2-57/60. e-f) tremolite and chlorite alteration in the troctolitic gabbro 92R2-72/75 tremolite and iron-oxide are just visible on the edges of the olivine grain in part e (see also Fig 2e,f).

Fig 4 Kendrick et al., 2022

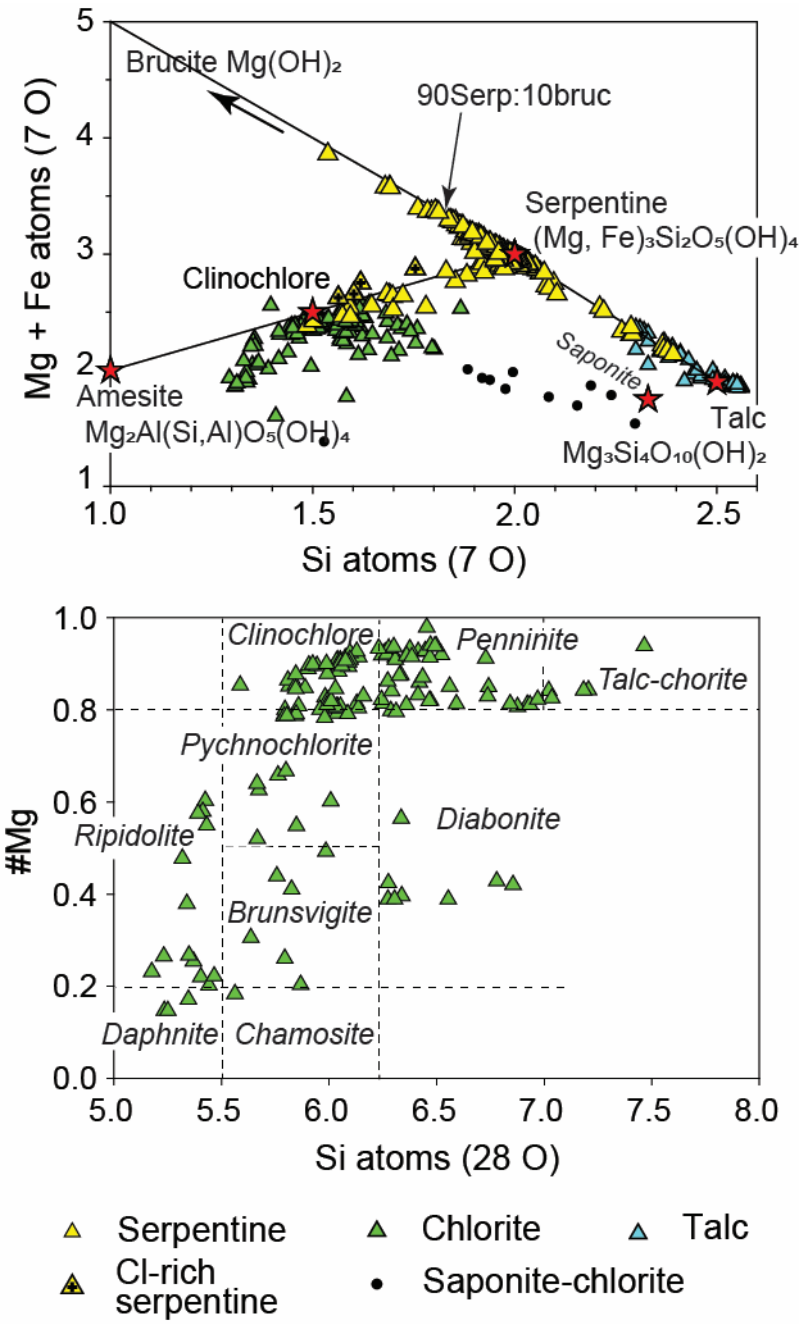

Fig 4. Major element data for the major Fe-Mg phylosilicates. a) atomic Mg + Fe versus Si per 7 O for phyllosilicates , showing mineral endmember compositions. Serpentine defines a vector toward brucite and vectors toward talc and either amesite or chlorite in some samples: the most Cl-rich serpentine analyses with 0.8-1.2 wt. % Cl are shown. Chlorite is also perturbed toward saponite demonstrating nano-scale intergrowth of phyllosilicates. b) atomic #Mg [Mg/(Mg +Fe)] versus Si diagram for chlorite classification after (Foster, 1962) assuming all Fe is Fe^{2+}.

Fig 5, Kendrick et al., 2022

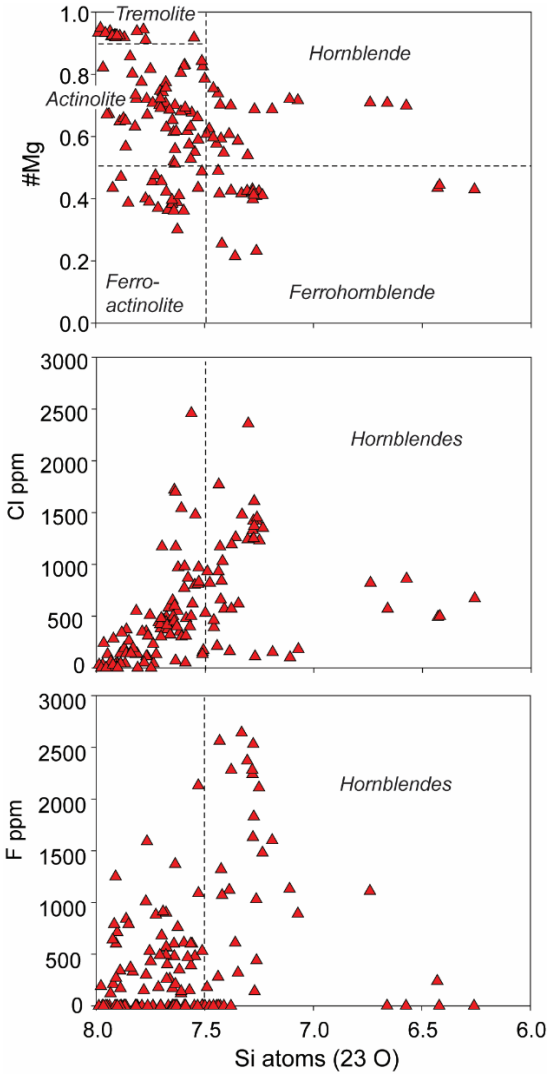

Fig 5. Amphiboles in Hole U1309D lithologies showing amphibole classification and halogen concentrations in µg/g as a function of Si atoms. Tremolites and actinolites tend to have lower concentrations of Cl than Ti-rich hornblendes, however, actinolites as well as hornblendes can have high F concentrations.

Fig 6, Kendrick et al., 2022

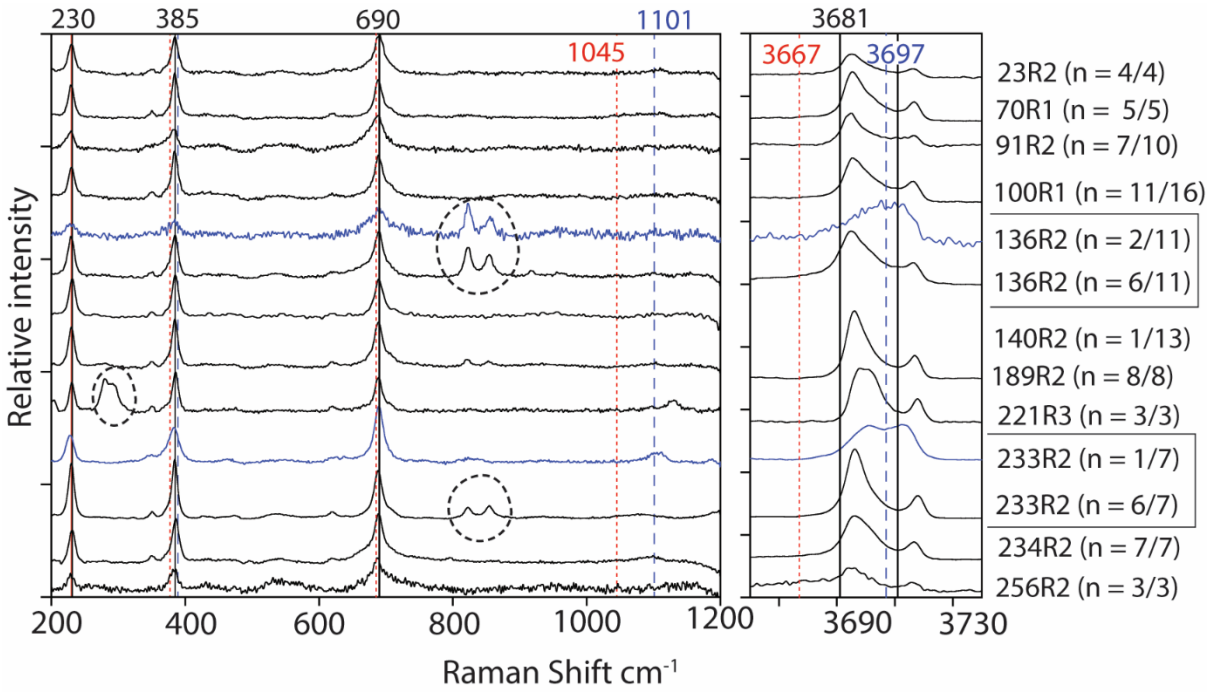

Fig 6. Raman spectra for serpentine polymorphs in Hole U1309D lithologies. Each spectrum shows relative intensity and is the sum of several similar spectra Vertical solid, dashed or dotted lines show the positions of characteristic peaks for lizardite (solid black lines), chrysotile (dashed blue lines) and antigorite (dotted red lines). Interferences indicating contaminant minerals are highlighted with dashed circles and reflect the presence of olivine (twin peaks at ~840 cm^{-1}) in 136R2-57/60 and 233R2-70/73; and an unidentified mineral (possibly sulphide) in 221R3-100/102.

Fig 7, Kendrick et al., 2022

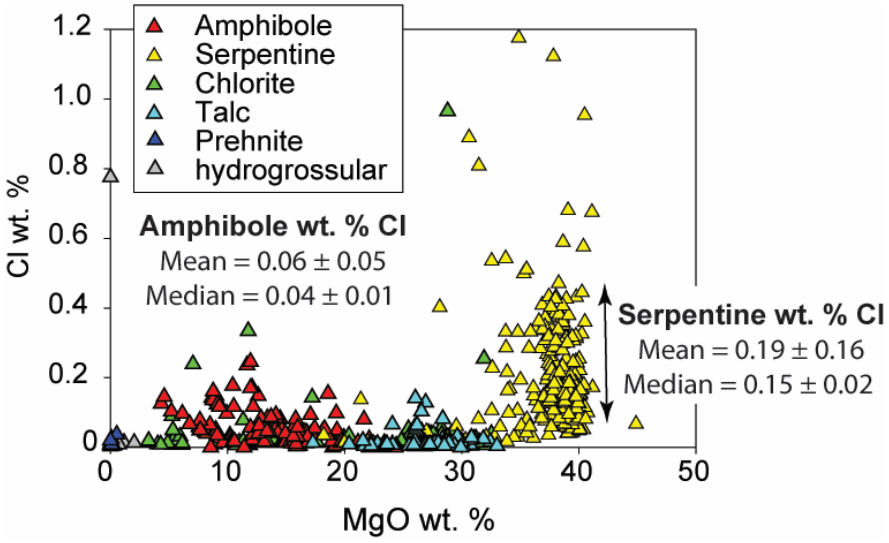

Fig 7. Plot showing the range of Cl concentrations in common alteration minerals separated on the basis of MgO. Serpentine has by far the highest average Cl concentration followed by hornblende. Tremolite, actinolite, chlorite and talc have much lower concentrations of 10-100s µg/g Cl.

Fig 8, Kendrick et al., 2022

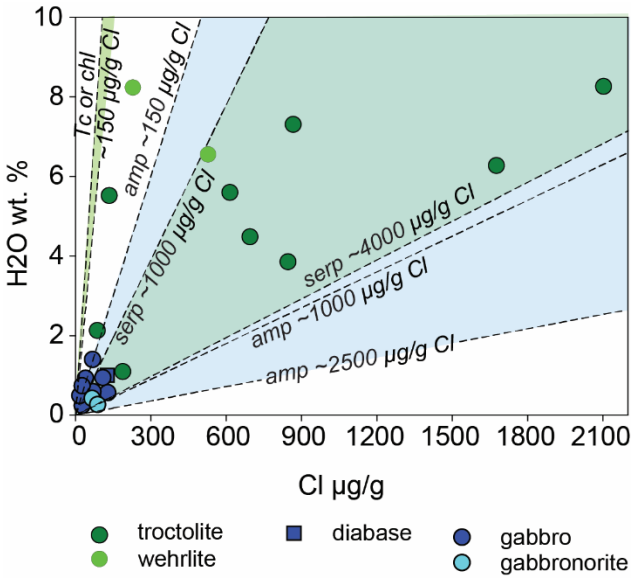

Fig 8. Whole rock Cl and H_2O concentrations. The slopes represent the estimated ranges of H_2O/Cl in the dominant alteration minerals with the observed ranges of Cl concentration. Serpentine is the dominant alteration mineral in troctolites and olivine-rich troctolites and the most Cl-rich samples contain Cl-rich serpentine.

Fig 9, Kendrick et al., 2022

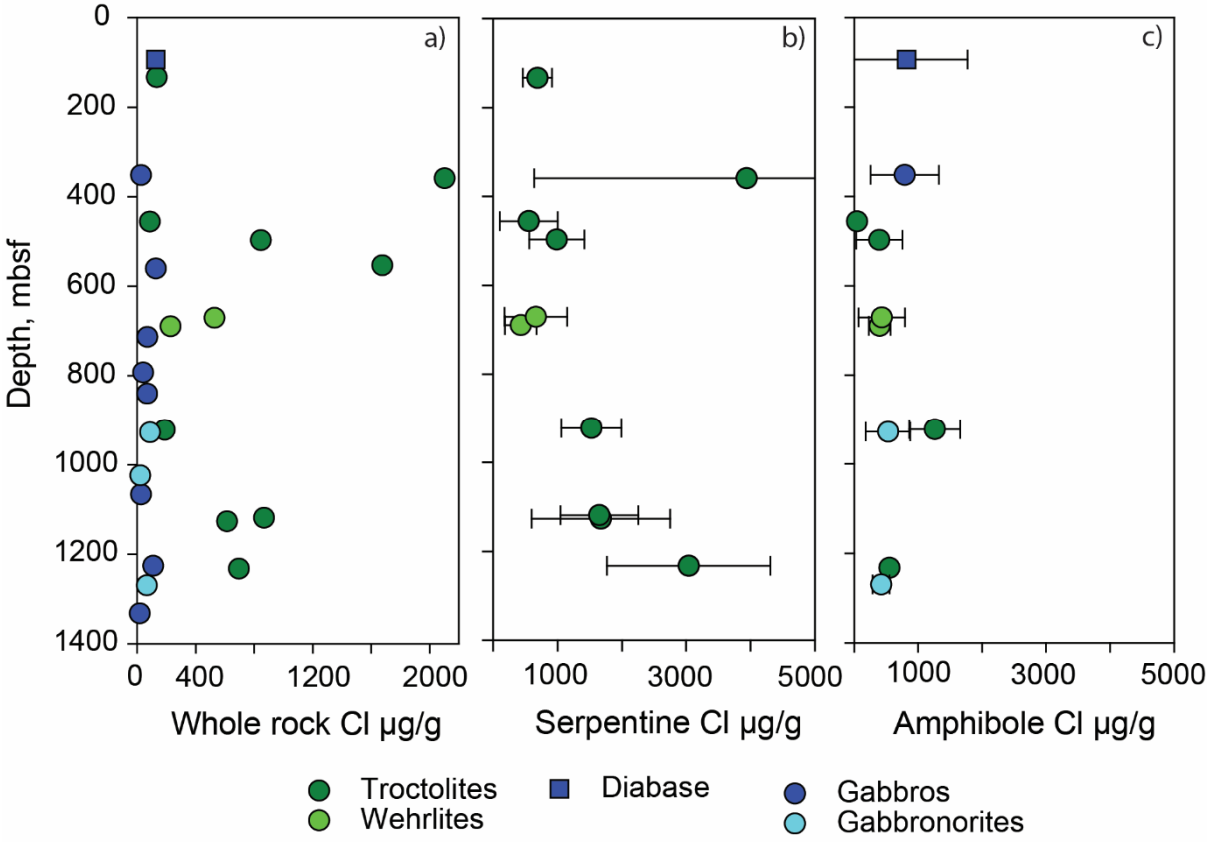

Fig 9. Downhole variation in Cl concentration of Hole U1309D lithologies and minerals: a) whole rocks, b) serpentine and c) amphibole. The standard deviation of electron microprobe analyses is shown in parts b and c. The concentration of Cl is related to the abundance of olivine-rich lithologies, not depth down the hole.

Fig 10, Kendrick et al., 2022

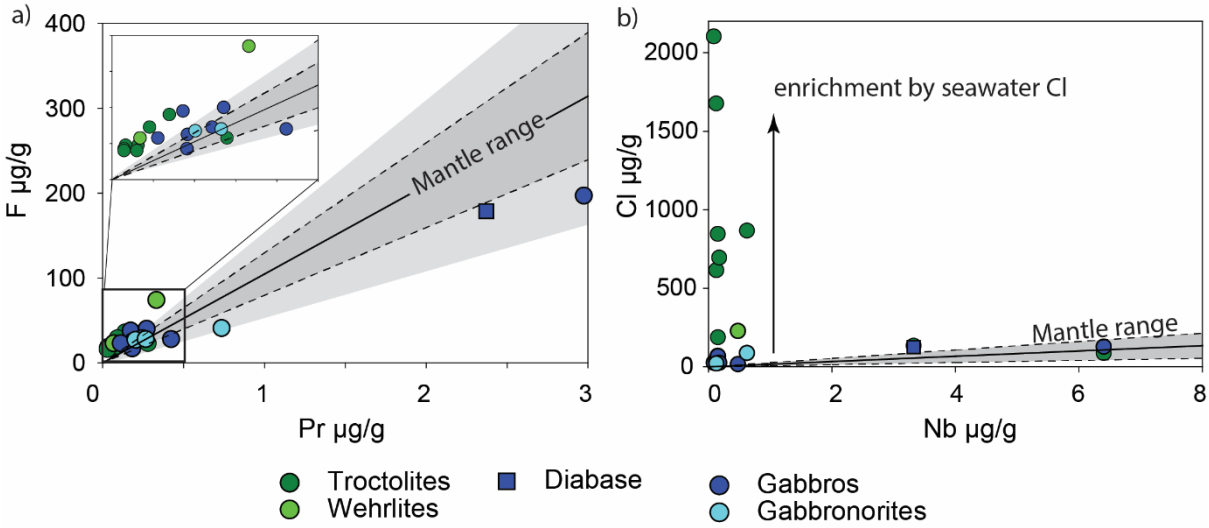

Fig 10. Plots showing the relative enrichment of F and Cl: a) F vs Pr and b) Cl versus Nb. The shaded envelopes show F/Pr and Cl/Nb ratios typical of MORB glasses, which represent unaltered ocean crust. The plots show olivine-rich lithologies are slightly enriched in F, while the gabbros are not. The olivine-rich lithologies are ~11 times more enriched in Cl than the gabbos.

Fig 11, Kendrick et al., 2022

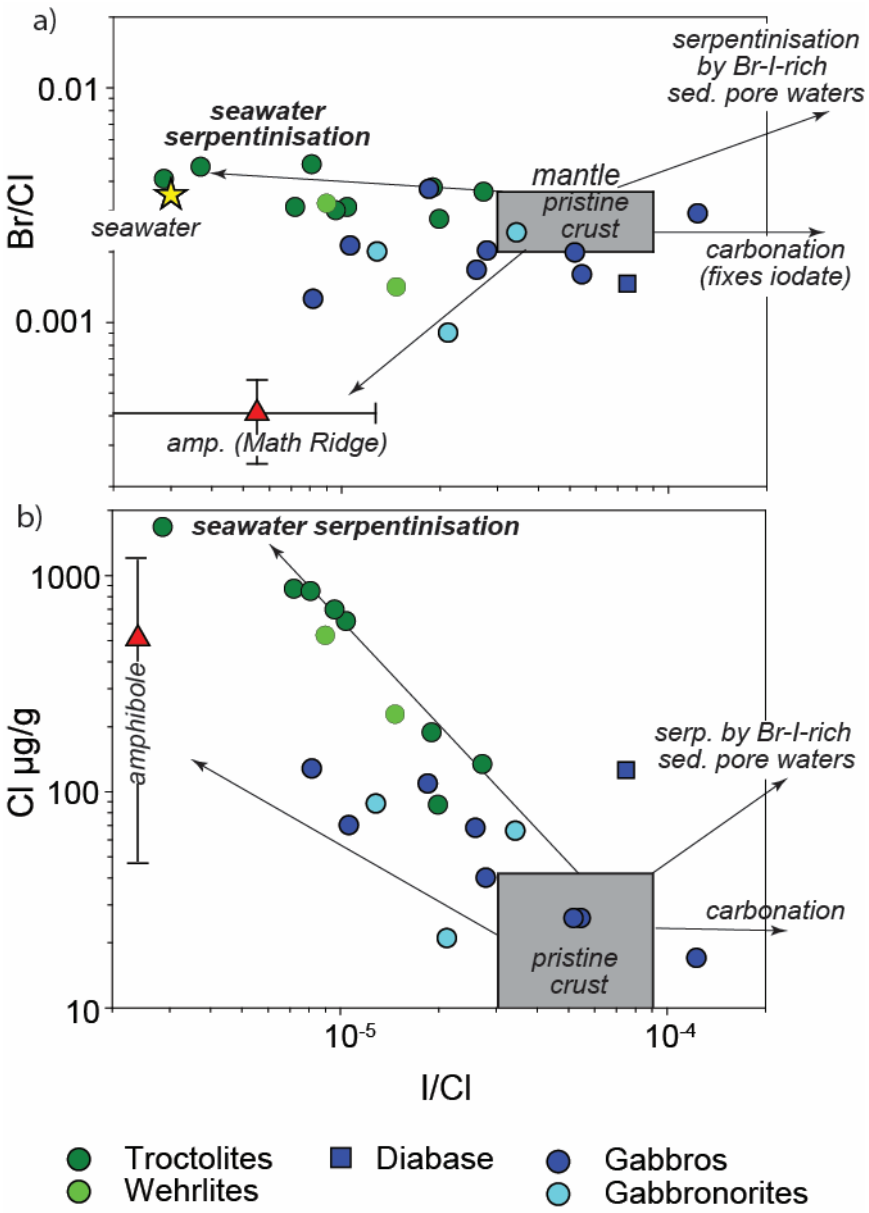

Fig 11. Halogen data for Hole U1309D troctolites and gabbros. a) a log-log Br/Cl versus I/Cl plot showing reference fields for the mantle (Kendrick et al., 2017), amphibole (Kendrick et al., 2015a) and seawater. b) log-log I/Cl versus Cl µg/g showing estimated reference fields for pristine crust with mantle I/Cl ratio and average amphiboles. The data define trends that can be explained by adding Cl-rich amphibole and serpentine to the pristine crustal lithologies. Vectors for the styles of alteration investigated in this and previous studies of ophiolitic/forearc serpentinites (Kendrick et al., 2013b) and oxidised carbonate-alteration (Kendrick, 2019b; Kendrick et al., 2020a) are shown for reference.

Fig 12, Kendrick et al., 2022

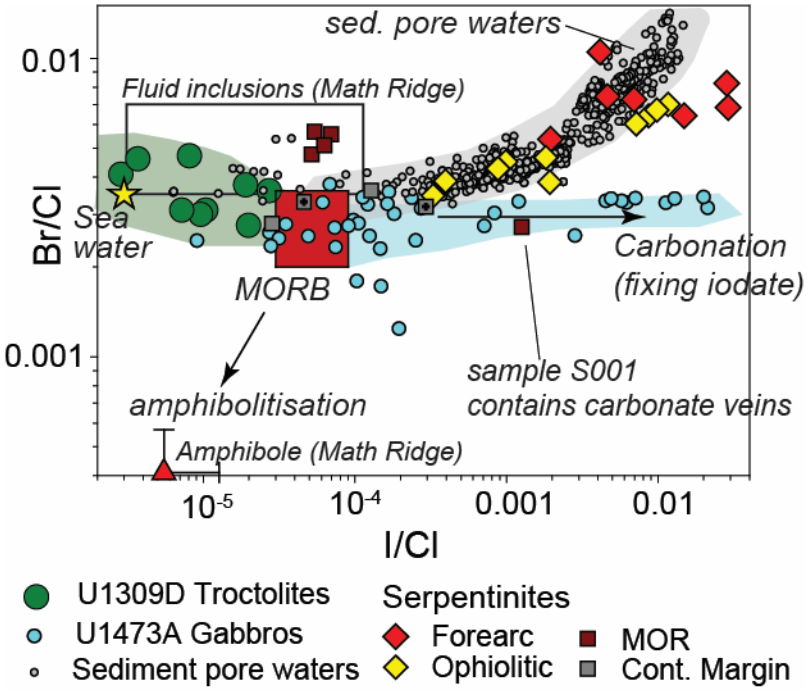

Fig 12. Log-log Br/Cl versus I/Cl plot showing the serpentinised-troctolites and olivine-rich troctolites of this study together with previous studies of serpentinites (Kendrick et al., 2013b) and altered gabbros from Hole U1473A, which are strongly altered by carbonate and iron oxyhydroxides (Kendrick, 2019b; Kendrick et al., 2020a). Sedimentary pore waters (e.g. Fehn et al., 2006; Muramatsu et al., 2007; Tomaru et al., 2007), the MORB mantle field (Kendrick et al., 2017), and fluid inclusions and amphibole from the Mathematician Ridge are shown for reference (Kendrick et al., 2015a). The high I/Cl of serpentinite sample S001 is not typical of MOR serpentinites and is attributed here to the presence of carbonate-veins.

References

Beard, J.S., Frost, B.R., Fryer, P., McCaig, A., Searle, R., Idlefonse, B., Zinin, P., Sharma, S.K., 2009. Onset and progression of serpentinisation and magnetite formation in olivine-rich troctolite from IODP Hole U1309D. J. Petrol. 50, 387-403.

Blackman, D.K., Idlefonse, B., John, B.E., Ohara, Y., Miller, D.J., Macleod, C.J., Scientists, E., 2006. Proceedings of the Integrated Ocean Drilling Program. 304/305.

Blackman, D.K., Ildefonse, B., John, B.E., Ohara, Y., Miller, D.J., Abe, N., Abratis, M., Andal, E.S., Andreani, M., Awaji, S., Beard, J.S., Brunelli, D., Charney, A.B., Christie, D.M., Collins, J., Delacour, A.G., Delius, H., Drouin, M., Einaudi, F., Escartin, J., Frost, B.R., Fruh-Green, G., Fryer, P.B., Gee, J.S., Godard, M., Grimes, C.B., Halfpenny, A., Hansen, H.E., Harris, A.C., Tamura, A., Hayman, N.W., Hellebrand, E., Hirose, T., Hirth, J.G., Ishimaru, S., Johnson, K.T.M., Karner, G.D., Linek, M., MacLeod, C.J., Maeda, J., Mason, O.U., McCaig, A.M., Michibayashi, K., Morris, A., Nakagawa, T., Nozaka, T., Rosner, M., Searle, R.C., Suhr, G., Tominaga, M., von der Handt, A., Yamasaki, T., Zhao, X., 2011. Drilling constraints on lithospheric accretion and evolution at Atlantis Massif, Mid-Atlantic Ridge 30 degrees N. J. Geophys. Res.-Solid Earth 116.

Boreham C.J., Sohn J.H., Cox N., Williams J., Hong Z., Kendrick M.A., 2021. Hydrogen and hydrocarbons associated with the Neoarchean Frog's Leg Gold Camp, Yilgarn Craton, Western Australia. Chemical Geology: 120098.Bostock, M.G., Hyndman, R.D., Rondenay, S., Peacock, S.M., 2002. An inverted continental Moho and serpentinization of the forearc mantle. Nature 417, 536-538.

Bradley, A. S. and Summons R.E., 2010. Multiple origins of methane at the Lost City Hydrothermal Field. Earth and Planetary Science Letters 297(1-2): 34-41.

Carmigano, O.R.D.R., Vieira, S.S., Brandao, P.R.G., Bertoli, A.C., Lago, R.M., 2020. Serpentinites: Mineral structure, properties and technological applications. Jouranl of Brazilian Chemical Society 31, 2-14.

Carter, E.J., O'Driscoll, B., Burgess, R., Clay, P.L., 2021. Multi-stage fluid infiltration and metasomatism in supra-subduction zone mantle: evidence from halogens and noble gases in the Leka Ophiolite Complex, Norway. Geochimica et Cosmochimica Acta 307, 258-280.

Castelain T., McCaig A.M., Cliff R.A., 2014. Fluid evolution in an Oceanic Core Complex: A fluid inclusion study from IODP hole U1309 D-Atlantis Massif, 30 degrees N, Mid-Atlantic Ridge. Geochemistry Geophysics Geosystems 15(4): 1193-1214.

Cathelineau, M., 1988. Cation site occupancy in chlorites and illites as a function of temperature. Clay Minerals 23, 471-485.

Cathelineau, M., Nieva, D., 1985. A chlorite solid-solution geothermometer – The Los-Azufres (Mexico) Geothermal System. Contributions to Mineralogy and Petrology 91, 235-244.

Chavrit, D., Burgess, R., Sumino, H., Teagle, D.A.H., Droop, G., Shimizu, A., Ballentine, C.J., 2016. The contribution of hydrothermally altered ocean crust to the mantle halogen and noble gas cycles. Geochimica et Cosmochimica Acta 183, 106-124.

Decaritat, P., Hutcheon, I., Walshe, J.L., 1993. CHLORITE GEOTHERMOMETRY - A REVIEW. Clays and Clay Minerals 41, 219-239.

Deschamps, F., Godard, M., Guillot, S., Hattori, K., 2013. Geochemistry of subduction zone serpentinites: A review. Lithos 178, 96-127.

Drever, J.I., 1997. The Geochemistry of Natural Waters: Surface and Groundwater Environments, 3rd ed. Prentice-Hall Inc., Upper Saddle River, New Jersey.

Drouin, M., Godard, M., Ildefonse, B., Bruguier, O., Garrido, C.J., 2009. Geochemical and petrographic evidence for magmatic impregnation in the oceanic lithosphere at Atlantis Massif, Mid-Atlantic Ridge (IODP Hole U1309D, 30 degrees N). Chemical Geology 264, 71-88.

Drouin, M., Ildefonse, B., Godard, M., 2010. A microstructural imprint of melt impregnation in slow spreading lithosphere: Olivine-rich troctolites from the Atlantis Massif, Mid-Atlantic Ridge, 30 degrees N, IODP Hole U1309D. Geochem. Geophys. Geosyst. 11.

Ernst, W.G., Liu, J., 1998. Experimental phase-equilibrium study of Al- and Ti-contents of calcic amphibole in MORB - A semiquantitative thermobarometer. Am. Miner. 83, 952-969.

Expedition 304/305 Scientists, 2006. Site U1309, in: Blackman, D.K., Idlefonse, B., John, B.E., Ohara, Y., Miller, D.J., MacLeod, C.J., Scientists, E. (Eds.), Proceedings of the IODP 304/305. Integrated Ocean Drilling Program Management International, Inc., College Station TX

Expedition 345 Scientists, 2013. Hess Deep plutonic crust: exploring the plutonic crust at a fast-spreading ridge: new drilling at Hess Deep, IODP Prel. Rept. 345, College Station TX.

Fehn, U., Lu, Z., Tomaru, H., 2006. 129I/I ratios and halogen concentrations in pore water of Hydrate Ridge and their relevence for the origin of gas hydrates: a progress report, in: Trehu, A.M., Bohrmann, G., Torres, M.E., Colwell, F.S. (Eds.), Proceedings of the Ocean Drilling Program, Scientific Results, pp. 1-25.

Foster, M.D., 1962. Interpretation of the Composition and a Classification of the Chlorites. United States Geological Survey Professional Paper 414-A, 1-33.

Frost, B.R., Beard, J.S., McCaig, A., Condliffe, E., 2008. The formation of micro-rodingites from IODP Hole 1309D: Key to understanding the process of serpentinisation. J. Petrol. 49, 1579-1588.

Godard, M., Awaji, S., Hansen, H., Hellebrand, E., Brunelli, D., Johnson, K., Yamasaki, T., Maeda, J., Abratis, M., Christie, D., Kato, Y., Mariet, C., Rosner, M., 2009. Geochemistry of a long in-situ section of intrusive slow-spreading oceanic lithosphere: Results from IODP Site U1309 (Atlantis Massif, 30 N Mid-Atlantic Ridge). Earth and Planetary Science Letters 279, 110-122.

Grevemeyer, I., Ranero, C.R., Ivandic, M., 2018. Structure of ocean crust and serpentinisation at subduction trenches. Geosphere 14, 395-418.

Hillier, S., Velde, B., 1991. Octehedral occupancy and the chemical composition of diagenetic (low temperature) chlorites. Clay Minerals 26, 149-168.

Hilton, D.R., Fischer, T.P., Marty, B., 2002. Noble Gases and Volatile Recycling at Subduction Zones, in: Porcelli, D., Ballentine, C., Wieler, R. (Eds.), Noble Gases in Geochemistry and Cosmochemistry. Mineralogical Society of America, Washington D.C., pp. 319-370.

Ito, E., Harris, D.M., Anderson, A.T., 1983. Alteration of Oceanic-Crust and Geologic Cycling of Chlorine and Water. Geochimica et Cosmochimica Acta 47, 1613-1624.

Jarrard, R.D., 2003. Subduction fluxes of water, carbon dioxide, chlorine, and potassium. Geochem. Geophys. Geosyst. 4.

Jenkins, D.M., 2019. The incorporation of chlorine into calcium amphibole. Am. Miner. 104, 514-524.

John, T., Scambelluri, M., Frische, M., Barnes, J.D., Bach, W., 2011. Dehydration of subducting serpentinite: Implications for halogen mobility in subduction zones and the deep halogen cycle. Earth and Planetary Science Letters 308, 65-76.

Kelley, D.S., Fruh-Green, G.L., Karson, J.A., Ludwig, K.A., 2007. The Lost City Hydrothermal Field Revisited. Oceanography 20, 90-99.

Kelley, D.S., Karson, J.A., Fruh-Green, G.L., Yoerger, D.R., Shank, T.M., Butterfield, D.A., Hayes, J.M., Schrenk, M.O., Olson, E.J., Proskurowski, G., Jakuba, M., Bradley, A., Larson, B., Ludwig, K., Glickson, D., Buckman, K., Bradley, A.S., Brazelton, W.J., Roe, K., Elend, M.J., Delacour, A., Bernasconi, S.M., Lilley, M.D., Baross, J.A., Summons, R.T., Sylva, S.P., 2005. A serpentinite-hosted ecosystem: The lost city hydrothermal field. Science 307, 1428-1434.

Kendrick, M.A., 2012. High precision Cl, Br and I determination in mineral standards using the noble gas method. Chemical Geology 292-293, 116-126.

Kendrick, M.A., 2019a. Halogens in altered ocean crust from the East Pacific Rise (ODP/IODP Hole 1256D). Geochimica et Cosmochimica Acta 261, 93-112.

Kendrick, M.A., 2019b. Halogens in Atlantis Bank gabbros, SW Indian Ridge: implications for styles of seafloor alteration. Earth and Planetary Science Letters 514, 96-107.

Kendrick, M.A., Arculus, R.J., Burnard, P., Honda, M., 2013a. Quantifying brine assimilation by submarine magmas: Examples from the Galápagos Spreading Centre and Lau Basin. Geochimica et Cosmochimica Acta 123, 150-165.

Kendrick, M.A., Arculus, R.J., Danyushevsky, L., Kamenetsky, V.S., Woodhead, J., Honda, M., 2014. Subduction-related halogens (Cl, Br and I) and H2O in magmatic glasses from Southwest Pacific Backarc Basins. Earth and Planetary Science Letters 400, 165-176.

Kendrick, M.A., Caulfield, J., Nguyen, A., Zhao, J.-X., Blakey, I., 2020a. Halogen and trace element analysis of carbonate-veins and Fe-oxyhydroxide by LA-ICPMS: implications for seafloor alteration on the Atlantis Bank, SW Indian Ridge Chemical Geology 547, 119668.

Kendrick, M.A., D'Andres, J., Holden, P., Ireland, T., 2018a. Halogens (F, Cl, Br, I) in thirteen USGS, GSJ and NIST international rock powder and glass reference materials. Geostandards and Geoanalytical Research 42, 499-511.

Kendrick, M.A., Danyushevsky, L., Falloon, T., Woodhead, J.D., Arculus, R., Ireland, T., 2020b. SW Pacific arc and backarc lavas and the role of slab-bend serpentinites in the global halogen cycle. Earth and Planetary Science Letters 530, 115921.

Kendrick, M.A., Hémond, C., Kamenetsky, V.S., Danyushevsky, L., Devey, C.W., Rodemann, T., Jackson, M.G., Perfit, M.R., 2017. Seawater cycled throughout Earth's mantle in partially serpentinized lithosphere. Nat. Geosci. 10, 222-228.

Kendrick, M.A., Honda, M., Pettke, T., Scambelluri, M., Phillips, D., Giuliani, A., 2013b. Subduction zone fluxes of halogens and noble gases in seafloor and forearc serpentinites. Earth and Planetary Science Letters 365, 86-96.

Kendrick, M.A., Honda, M., Vanko, D.A., 2015a. Halogens and noble gases in Mathematician Ridge meta-gabbros, NE Pacific: implications for oceanic hydrothermal root zones and global volatile cycles. Contributions to Mineralogy and Petrology 170, 1-20.

Kendrick, M.A., Jackson, M.G., Hauri, E., Phillips, D., 2015b. The halogen (F, Cl, Br, I) and H2O systematics of Samoan lavas: Assimilated seawater, EM2 and high 3He/4He components Earth and Planetary Science Letters 410, 197-209.

Kendrick, M.A., Scambelluri, M., Hermann, J., Padrón-Navarta, J.A., 2018b. Halogens and noble gases in serpentinites and secondary peridotites: Implications for seawater subduction and the origin of mantle neon. Geochimica et Cosmochimica Acta 235, 285-304.

Kendrick, M.A., Scambelluri, M., Honda, M., Phillips, D., 2011. High abundances of noble gas and chlorine delivered to the mantle by serpentinite subduction. Nat. Geosci. 4, 807-812.

Klein, F., Bach, W., Humphris, S.E., Kahl, W.A., Jons, N., Moskowitz, B., Berquo, T.S., 2014. Magnetite in seafloor serpentinite-Some like it hot. Geology 42, 135-138.

Kodolányi, J., Pettke, T., Spandler, C., Kamber, B.S., Gméling, K., 2012. Geochemistry of Ocean Floor and Fore-arc Serpentinites: Constraints on the Ultramafic Input to Subduction Zones. J. Petrol. 53, 235-270.

Kullerud, K., 1996. Chlorine-rich amphiboles: Interplay between amphibole composition and an evolving fluid. European Journal of Mineralogy 8, 355-370.

le Roux, P.J., Shirey, S.B., Hauri, E.H., Perfit, M.R., Bender, J.F., 2006. The effects of variable sources, processes and contaminants on the composition of northern EPR MORB (8-10 degrees N and 12-14 degrees N): Evidence from volatiles (H2O, CO2, S) and halogens (F, Cl). Earth and Planetary Science Letters 251, 209-231.

Le Voyer, M., Cottrell, E., Kelley, K.A., Brounce, M., Hauri, E.H., 2015. The effect of primary versus secondary processes on the volatile content of MORB glasses: An example from the equatorial Mid-Atlantic Ridge (5 degrees N-3 degrees S). J. Geophys. Res.-Solid Earth 120, 125-144.

Marschall, H.R., Schumacher, J.C., 2012. Arc magmas sourced from mélange diapirs in subduction zones. Nat. Geosci. 5, 862-867.

Muramatsu, Y., Doi, T., Tomaru, H., Fehn, U., Takeuchi, R., Matsumoto, R., 2007. Halogen concentrations in pore waters and sediments of the Nankai Trough, Japan: Implications for the origin of gas hydrates. Applied Geochemistry 22, 534-556.

Nielsen, S.G., Marschall, H.R., 2017. Geochemical evidence for melange melting in global arcs. Science Advances 3, e1602402.

Nozaka, T. and Fryer P., 2011. Alteration of the Oceanic Lower Crust at a Slow-spreading Axis: Insight from Vein-related Zoned Halos in Olivine Gabbro from Atlantis Massif, Mid-Atlantic Ridge. Journal of Petrology 52(4): 643-664.

Nozaka, T., Wintsch, R.P., Meyer, R., 2017. Serpentinization of olivine in troctolites and olivine gabbros from the Hess Deep Rift. Lithos 282, 201-214.

Ohtani, E., 2020. Hydration and Dehydration in Earth's Interior. Annual Review of Earth and Planetary Sciences.

Pagé, L., Hattori, K., 2017. Tracing halogen and B cycling in subduction zones based on obducted, subducted and forearc serpentinites of the Dominican Republic. Scientific Reports 7.

Pagé, L., Hattori, K., 2019. Abyssal Serpentinites: Transporting Halogens from Earth’s Surface to the Deep Mantle. Minerals 9, 61.

Pagé, L., Hattori, K., Guillot, S., 2018. Mantle wedge serpentinites: A transient reservoir of halogens, boron, and nitrogen for the deeper mantle. Geology 46, 883-886.

Pearce, J., Stern, R.J., 2006. Origin of Back-Arc Basin Magmas: Trace Element and Isotope Perspectives, Back-arc Spreading Systems: Geological, Biological, Chemical and Physical Interactions. American Geophysical Union, pp. 63-86.

Plümper, O., Røyne, A., Magrasó, A., Jamtveit, B., 2012. The interface-scale mechanism of reaction-induced fracturing during serpentinization. Geology 40, 1103-1106.

Ranero, C.R., Phipps Morgan, J., McIntosh, K., Reichert, C., 2003. Bending-related faulting and mantle serpentinization at the Middle America trench. Nature 425, 367-373.

Roddick, J.C., 1983. High precision intercalibration of 40Ar-39Ar standards. Geochimica et Cosmochimica Acta 47, 887-898.

Roumejon, S., Fruh-Green, G.L., Orcutt, B.N., Party, I.E.S., 2018. Alteration Heterogeneities in Peridotites Exhumed on the Southern Wall of the Atlantis Massif (IODP Expedition 357). J. Petrol. 59, 1329-1357.

Rüpke, L.H., Morgan, J.P., Hort, M., Connolly, J.A.D., 2004. Serpentine and the subduction zone water cycle. Earth and Planetary Science Letters 223, 17-34.

Scambelluri, M., Fiebig, J., Malaspina, N., Müntener, O., Pettke, T., 2004. Serpentinite Subduction: Implications for Fluid Processes and Trace-Element Recycling. International Geology Review 46, 595-613.

Scambelluri, M., Müntener, O., Hermann, J., Piccardo, G.B., Trommsdorff, V., 1995. Subduction of water into the mantle - History of an Alpine Peridotite Geology 23, 459-462.

Schroeder, T., Bach, W., Jons, N., Jons, S., Monien, P., Klugel, A., 2015. Fluid circulation and carbonate vein precipitation in the footwall of an oceanic core complex, Ocean Drilling Program Site 175, Mid-Atlantic Ridge. Geochem. Geophys. Geosyst. 16, 3716-3732.

Seyfried, W.E., Ding, K., 1995. The hydrothermal chemistry of fluoride in seawater. Geochimica et Cosmochimica Acta 59, 1063-1071.

Sharp, Z.D., Barnes, J.D., 2004. Water-soluble chlorides in massive seafloor serpentinites: a source of chloride in subduction zones. Earth and Planetary Science Letters 226, 243-254.

Starr, P.G., Pattison, D.R.M., Ames, D.E., 2020. Mineral assemblages and phase equilibria of metabasites from the prehnite–pumpellyite to amphibolite facies, with the Flin Flon Greenstone Belt (Manitoba) as a type example. 38, 71-102.

Svensen, H., Banks, D.A., Austreim, H., 2001. Halogen contents of eclogite facies fluid inclusions and minerals: Caledonides, western Norway. Journal of Metamorphic Geology 19, 165-178.

Tarling, M.S., Rooney, J.S., Viti, C., Smith, S.A.F., Gordon, K.C., 2018. Distinguishing the Raman spectrum of polygonal serpentine. 49, 1978-1984.

Ternieten, L., Früh-Green, G.L., Bernasconi, S.M., 2021. Distribution and Sources of Carbon in Serpentinized Mantle Peridotites at the Atlantis Massif (IODP Expedition 357). J. Geophys. Res.-Solid Earth 126.

Tomaru, H., Fehn, U., Lu, Z.L., Matsumoto, R., 2007. Halogen systematics in the Mallik 5L-38 gas hydrate production research well, Northwest Territories, Canada: Implications for the origin of gas hydrates under terrestrial permafrost conditions. Applied Geochemistry 22, 656-675.

Tonarini, S., Leeman, W.P., Leat, P.T., 2011. Subduction erosion of forearc mantle wedge implicated in the genesis of the South Sandwich Island (SSI) arc: Evidence from boron isotope systematics. Earth and Planetary Science Letters In Press, Corrected Proof.

Ulmer, P., Trommsdorff, V., 1995. Serpentine Stability to Mantle Depths and Subduction-Related Magmatism. Science 268, 858-861.

Volfinger, M., Robert, J.L., Vielzeuf, D., Neiva, A.M.R., 1985. Structural control of the chlorine content of OH-bearing silicates (micas and amphiboles). Geochimica et Cosmochimica Acta 49, 37-48.

Yoshida, K., Okamoto, A., Shimizu, H., Oyanagi, R., Tsuchiya, N., Party, O.D.P.P.S., 2020. Fluid Infiltration Through Oceanic Lower Crust in Response to Reaction-Induced Fracturing: Insights From Serpentinized Troctolite and Numerical Models. Journal of Geophysical Research: Solid Earth 125, e2020JB020268.